EUROPEAN ORGANIZATION FOR NUCLEAR RESEARCH

CERN-EP/88-75
23 June 1988

A HYBRID EXPERIMENT TO SEARCH FOR BEAUTY PARTICLES

S. Aoki[10], R. Arnold[5,a], G. Baroni[12], M. Barth[4], J.H. Bartley[9], D. Bertrand[4], G. Bertrand-Coremans[4], V. Bisi[15], A.C. Breslin[6], G. Carboni[5,b], M.G. Catanesi[3], A.M. Cecchetti[12], E. Chesi[5], K. Chiba[10], M. Coupland[8], D.H. Davis[9], S. Dell'Uomo[12], M. De Vincenzi[12], S. Di Liberto[12], W. Donnelly[6], B.G. Duff[9,†], M.J. Esten[9], A. Frenkel[12], D. Gamba[15], C. Gerke[5,c], P. Giubellino[15], M. Hazama[2], F.F. Heymann[9], K. Hoshino[10], D.C. Imrie[9,d], Y. Isokane[11], T. Kaway[10], M. Kazuno[14], M. Kobayashi[10], K. Kodama[10], G.J. Lush[9], Y. Maeda[17], A. Manfredini[12], G. Marini[12], G. Martellotti[12], A. Marzari-Chiesa[15], M.A. Mazzoni[12,e], F. Meddi[12], F. Minakawa[14], M. Miyanishi[10], A. Montwill[6], M.T. Muciaccia[3], P. Musset[5,†], M. Nakamura[10], Y. Nakamura[10], K. Nakazawa[7], S. Natali[3], A. Nigro[12], K. Niu[10], K. Niwa[10], S. Nuzzo[3], M. Ohashi[10], G. Penso[12], P. Pistilli[12,f], F. Piuz[5], G. Poulard[5], L. Ramello[15], L. Riccati[15], G. Romano[13], R. Roosen[4], G. Rosa[12], F. Ruggieri[3], H. Sasaki[10], Y. Sato[16], A. Sciubba[12], C. Sgarbi[12], H. Shibuya[14], S. Simone[3], H.I. Sletten[5], H. Tajima[10], S. Tasaka[7], I. Tezuka[16], Y. Tomita[10], D.N. Tovee[9], P. Trent[8], Y. Tsuneoka[11], N. Ushida[1], S. Watanabe[14], O. Yamakawa[10] and Y. Yanagisawa[10]

(Submitted to Nuclear Instruments and Methods in Physics Research)

---

1) Aichi University of Education, Kariya, Japan.
2) Aichi Women's College, Nisshin-Chyo, Aichi, Japan.
3) Dipartimento di Fisica dell'Università and INFN, Bari, Italy.
4) Inter-University Institute for High Energies, ULB-VUB, Brussels, Belgium.
5) CERN, Geneva, Switzerland.
6) Department of Physics, University College Dublin, Ireland.
7) Faculty of Education, Gifu University, Japan.
8) Birkbeck College, London, UK.
9) Department of Physics and Astronomy, University College London, UK.
10) Department of Physics, Nagoya University, Japan.
11) Nagoya Institute of Technology, Japan.
12) Dipartimento di Fisica, Università La Sapienza and INFN, Rome, Italy.
13) Dipartimento di Fisica Teorica e SMSA, and INFN, Salerno, Italy.
14) Department of Physics, Toho University, Funabashi, Japan.
15) Dipartimento di Fisica Sperimentale dell'Università and INFN, Turin, Italy.
16) Faculty of Education, Utsunomiya University, Japan.
17) Faculty of Education, Yokohama National University, Japan.

Present addresses:
a) CRN and Université Louis Pasteur, Strasburg, France.
b) INFN, Pisa, Italy.
c) DESY, Hamburg, Fed. Rep. Germany.
d) Brunel University, Uxbridge, UK.
e) CERN, Geneva, Switzerland.
f) University and INFN, Lecce, Italy.
†) Deceased.

ABSTRACT

We give here a detailed description of experiment WA75, which was performed at CERN to search for beauty particles. Events containing at least one muon with a high momentum transverse to the beam direction were selected; then the primary interactions and decay vertices, located in stacks of nuclear research emulsions, were examined and analysed. The various parts of the apparatus are described and the off-line analysis and search in emulsion are discussed. An estimate is made of the sensitivity of the experiment to beauty- and charmed-particle production.

1. INTRODUCTION

The apparatus described in this paper was designed [1] to search for direct evidence of the production and decay of beauty particles produced by a beam of π^- mesons of 350 GeV/c momentum.

The signal was selected from events of the kind

$$\pi^- N \rightarrow \mu^{\pm} + X$$

by requiring a high component (p_T) of the muon momentum (p), transverse to the beam direction. This is a typical signature of the semileptonic decay

$$B \rightarrow \mu^{\pm} + Y ,$$

which has a branching ratio BR = (11.0 ± 0.9%) [2]. As the decay of beauty particles into charmed particles dominates other decay modes [2], one requires, as unambiguous evidence of the production and subsequent decay of beauty particles, the direct observation of at least three, and preferably four, decay vertices in the corresponding sequences:

$$\begin{array}{l} B + \bar{B} \rightarrow \bar{C} + \ldots \\ \quad \hookrightarrow C + \ldots \hookrightarrow \ldots \\ \quad\quad \hookrightarrow \ldots \end{array}$$

The muon (or muons) may be present at any decay vertex, but of course those from beauty-particle decay usually have a higher p and p_T. This set of criteria, whilst retaining a good fraction of the signal, minimizes the background. Up to now, one clear example of such a chain of decays has been found [3], in an event containing two like-sign muons. In the course of the same search, two events, showing the double associated production of charmed particles, have also been reported [4].

Nuclear emulsions were chosen as an active target because of their high spatial resolution, providing sensitivity to short lifetimes and facilitating the analysis of events with several secondary vertices.

Experiment WA75 took data in 1983 and 1984 at CERN. The apparatus, sketched in fig. 1, comprised a beam hodoscope, emulsion stacks (mounted on a stage, moved during the beam spill), a vertex detector, an iron/tungsten dump, a magnetic spectrometer, and suitable trigger and data-acquisition systems. In the 1984 run, the dump was replaced by a hadron calorimeter; this is described elsewhere [5]. In the new configuration, and with a modified trigger, a search for supersymmetric particles was also performed [6].

The WA75 hybrid emulsion–counter system, and the acquisition and analysis of data, will be described in detail in the following sections. The emulsions and the target mover are dealt with in section 2; in section 3, the beam and dump; sections 4 and 5 cover the beam hodoscope, vertex detector, and magnetic spectrometer; section 6, the trigger and data acquisition, and section 7, the off-line analysis. The search in emulsion is described in section 8, the 1984 run in section 9, and acceptance and sensitivity in section 10.

2. EMULSIONS AND TARGET MOVER

2.1 Emulsions

A total of about 80 litres of nuclear emulsion, in the form of double-coated sheets and stripped pellicles, was irradiated in 1983 and 1984. The emulsions were exposed, with the beam either

perpendicular to, or parallel with, the emulsion surface, to exploit the advantages offered by the two approaches. Emulsions held perpendicular to the beam ('vertical') can tolerate higher track densities, whereas those held parallel ('horizontal') are more sensitive to very short lifetimes.

The emulsion was delivered in gel form by Fuji (75 litres of ET-7B) and Ilford (5 litres of G5). In order to produce the pellicles and sheets within a short time interval before the exposure, and also to save more than 50% of the current cost of ready-prepared emulsions, a pouring plant was built at CERN [7]. This is now a permanent facility, capable of producing up to two litres of dry emulsion per day. The sensitivity and overall quality of the emulsion proved to be excellent, and the sensitive material was stored, whenever necessary, within iron shielding.

Each vertical stack comprised 25 double-coated sheets (330 μm thick emulsion, coated on both sides of a 70 μm thick Lexan support), 25 cm $\times$ 25 cm in size (fig. 2) and packed in vacuum. In total, about 50 litres of emulsion was prepared in this form. The horizontal stacks (fig. 3) each comprised about 60 stripped emulsion pellicles, 11 cm $\times$ 4 cm (4 cm along the beam) and 600 μm thick, piled up and clamped between two rigid Perspex plates. Reference holes in each base-plate allowed the stacks to be located in exactly the same position, during both the subsequent exposure and the exposure to X-rays. Thin emulsions, already poured onto glass plates, were fixed to the stack-holders for intercalibration purposes.

The processing was carried out contemporaneously in Nagoya (for double-coated sheets), in Rome (for pellicles), and at CERN, where a new facility to develop double-coated sheets was built, for both. After processing, each double-coated sheet was cut into 64 squares, 3 cm $\times$ 3 cm in size. The corresponding 25 squares of a 'module' were then stuck, in sequence, on a single Lucite sheet. With this technique, the corresponding areas of consecutive emulsion sheets are adjacent, and the time needed to search for events and to follow tracks through the stack is greatly reduced [8]. The pellicles exposed horizontally were mounted on glass plates, then processed in the usual manner.

In order to provide a very accurate reference system within each vertical stack, grids were printed on one surface of each of the emulsion pellicles before processing. In addition to such a grid, a set of very thin X-ray marks [9] were used in the case of the horizontal stacks.

2.2 Target mover

The dimensions of the beam were small (see section 3) and it was therefore necessary to move the emulsions during each beam spill to give uniform irradiation. The target mover, shown in fig. 4, consisted of two vertical rails supported by a module which moved horizontally along another rail fixed to the base. The stacks were mounted on frames (six per frame, in the case of the horizontal ones) designed to glide along the vertical rails. The stage was driven by two d.c. motors controlled by a microcomputer, and the position of the target was read, in units of 2.5 μm, by means of linear encoders. The movement across the accessible area of 44 cm (horizontal) by 26.5 cm (vertical), including the out-of-beam position, proved to be accurate to $\sim$ 10 μm. The maximum speeds, with full load, were 30 and 15 mm/s along the vertical and horizontal directions, respectively. During the beam spill the target was moved only vertically to prevent small oscillations.

The local control system, based on a microprocessor, monitored the beam structure by integrating the beam intensity every 100 ms and changing the speed of the stage accordingly (to achieve uniform irradiation). The position of the stage was read by a CAMAC module.

3. BEAM AND DUMP

The experiment was installed in the H3 beam line in the CERN Super Proton Synchrotron (SPS) West Area, which provided a π^- beam of momentum 350 ($\pm$ 1%) GeV/c, with a 2 s beam spill and 12 s cycle. Beam-particle intensities of between 10^4 and 2 $\times$ 10^5 pions per burst were used. The optimum beam spot was of slightly elliptical shape (fig. 5), with its major axis perpendicular to the

motion of the emulsion. The r.m.s. spread in this projection was about 1.2 mm. This represented a compromise between the conflicting demands of providing a uniform track density in the emulsion and of ensuring that a large fraction of secondary particles should traverse the microstrip silicon detectors. Final steering, tuning, and subsequent monitoring were done using information from the microstrip silicon detectors.

The dump, built of iron blocks, had a total length of 2 m along the beam ($\sim 12\lambda_{abs}$), and was equipped with a central conical tungsten core ($\sim 20\lambda_{abs}$) of 25 mrad half angle. The tungsten was very effective in stopping the most energetic hadron showers, but had very little influence on the acceptance because of a small-angle veto behind it (see section 6) and the requirement of a high p_T. The fraction of events with punch-through tracks, removed by the subsequent shielding walls, was 2%, and constituted a negligible fraction of the events containing one or more muons.

4. BEAM HODOSCOPE AND VERTEX DETECTOR

The beam hodoscope (BH) and vertex detector (VD) were designed to provide the precise location of the interaction vertex in the emulsion stacks, and to reconstruct the topology of the outgoing secondary tracks. In addition, as emulsions have an 'infinite' memory, the VD was also expected to discriminate between topologies resulting from the decay of neutral particles which were associated with the primary vertex and those which were not. The VD was made as a compact array, 1 m long, to minimize the number of π and K decays into muons before the dump—the main source of background in this experiment.

Altogether, the two systems included 16 planes of microstrip silicon detectors (MSDs) and 16 planes of multiwire proportional chambers (MWPCs) (fig. 6); their geometrical characteristics are summarized in table 1. The MWPCs of the VD, being identical to those used in the muon spectrometer, will be described in section 5. The system of MSDs has been widely reported elsewhere [10]; here only the main features will be described.

The MSDs were built from 300 μm thick silicon wafers, using the process of passive-ion implantation [11]; different kinds were used, with pitches ranging from 50 μm to 200 μm (table 1).

Alignment of the BH and VD elements to within a few microns was necessary for good event reconstruction. Therefore (fig. 6), a granite table (T) was used as a master reference, on which two smaller granite blocks (B1 and B2) were aligned, one supporting the beam hodoscope, the other the microstrip detectors of the VD. The target mover (TM) was placed between the blocks. The bases supporting the BH and VD were put in position by using three steel spheres set on corresponding supports on the granite blocks, and the final mechanical alignment was done *in situ* by adjusting micromanipulators. The BH could be removed easily to permit the stacks to be changed at the end of each exposure.

The temperature in the entire target zone was kept at (12 $\pm$ 1)°C, both for mechanical stability and for the prevention of fading in the emulsions.

An analog readout chain was developed for the MSDs, to permit continuous monitoring of the stability of each channel and to provide pulse-height information. As no fast triggering was required from the MSDs, a multiplexed readout was developed for minimizing the number of ADC channels needed (one for each group of 32 strips). The MSDs were characterized by a typical signal-to-noise ratio of $\sim$ 16, and the response of the electronics was linear, within 2%, over the full ADC range.

For the purposes of track reconstruction a 'software threshold' (ST) was defined for each strip, and strips which showed a pulse height exceeding ST were considered as 'hits'. Readings of pedestal, mean, and r.m.s. values were recorded every few hours with a special pulser trigger.

The efficiency of the detectors was measured using beam particles; typical values were $\sim$ 98%, with some detectors falling to $\sim$ 90% owing to a relatively high number of dead strips or electronic channels. The alignment of detector planes was also checked using beam tracks and off-line

corrections, from 10 μm to 50 μm, introduced for individual planes. The BH r.m.s. resolution turned out to be 14 μm, in good agreement with that predicted ($\sigma = 50/\sqrt{12}$ μm) from the size of the strips.

5. MAGNETIC SPECTROMETER

The detectors and the spectrometer provided information for the event trigger logic and for precise measurement of the trajectories of muons, filtered by the dump, for the off-line analysis. The muon spectrometer consisted of a 1.5 T, 2 m diameter, bipolar superconducting magnet of large aperture (2.8 m $\times$ 1 m), equipped with a system of drift chambers and MWPCs (fig. 1). The scintillation counter system used for the first-level trigger is described in section 6.

The upstream part of the spectrometer consisted of three small MWPCs and four drift chambers; the downstream part comprised three large MWPCs. The position of the chambers is shown in fig. 1, and their main characteristics and the wire orientations are summarized in table 2. The cell design of the drift chambers was standard; staggering was applied to minimize the effect of left–right ambiguity of the drift information in track reconstruction. The spatial resolution was 250 μm and the efficiencies were 94% for chamber 1 and 99% for the others. The MWPCs in front of the magnet, identical to those used in the VD, each consisted of four planes arranged in pairs, with orthogonal sets of anode wires. The wire spacing was 1 mm and the anode–cathode gap 5 mm. Two pairs of planes were mounted on each of three support plates. The efficiency was found to be higher than 99% across the whole useful area of all planes.

High voltage (2.5 kV) was provided by a 16-channel 7 kV unit, controlled by computer for setting and monitoring.

The large MWPCs behind the magnet were designed and built by the WA7 Collaboration and are described elsewhere [12]. The last two chambers were placed so as to have a 60 cm wire superposition in the central region, where the particle flux was maximum. Typical average cluster size was 1.3 wires, and the mean efficiency of the single planes was measured to be (92 $\pm$ 2)%.

The readout for the drift chambers was the CERN drift-time recorder (DTR) system [13], and for the MWPCs the CERN receiver-memory hybrid (RMH) system [14].

6. TRIGGER AND DATA ACQUISITION

The signature for $B\bar{B}$ associated production was taken to be the emergence of one or more muons from the dump. As events with two or more muons represent a small fraction of those with a single muon (dominated by π and K decays), the general philosophy of the on-line trigger was to cut single-muon events where the muon emerged at a small angle to the beam (small transverse momentum). A compromise between the conflicting requirements of a high event rate (optimizing the data-acquisition possibilities, but over-exposing the emulsion) and a reasonable exposure duration led to the choice of beam intensity quoted in subsection 6.3.

6.1 Trigger detectors

The various detectors which contributed to the trigger were as follows (figs. 1 and 6):

i) *Beam counters.* These comprised two separate, fast (~ 20 ns transit time) photomultiplier (PM) tubes, each viewing a separate plastic scintillator. The scintillators (~ 10 mm^2) were placed in sequence in the beam upstream of the BH, and the PM signal generated from the coincidence of both counters was used to give the DTR 'stop' signal (which read out the drift chambers) and to regulate the instantaneous speed of the TM.

ii) *Silicon beam counters.* These consisted of a sandwich of four silicon discs (BC in fig. 6) equipped with fast shaping preamplifiers and discriminators. The beam signal was derived by forming the analog sum of two pairs, then used, in coincidence, to generate a short hold to the MSD readout logic.

iii) *Interaction counters.* These were four silicon disk counters (IC in fig. 6), similar to those used for the beam counter. Each channel was discriminated separately, without prior formation of analog sums, and an interaction was defined to be the coincidence of all four counters, with the threshold usually set to about 2.5 times minimum ionization. The interaction signal could also be used for selective readout of the MSDs.

iv) *Hodoscope arrays (H1y, H1z, H2, H3).* These scintillator arrays, situated after the dump (fig. 1) were constructed from strips of scintillator, 5 cm wide and 1 cm thick, and had lateral dimensions such as to cover the overall spectrometer acceptance. They were used in the trigger logic.

v) *Small-angle veto (SAV).* This was a concentric array of four circular counters, of varying diameters, placed directly downstream from the muon filter. Their diameters were 14.4, 18, 21.5, and 25 cm, respectively, the last subtending a cone of opening angle 42 mrad, with its apex at the emulsion target. Any of these counters could be used in the trigger logic to veto events with a single muon emitted within a preset angle to the beam.

6.2 Trigger logic

Trigger processing was organized on two levels: i) a pretrigger (T0), based on a valid interaction in coincidence with one or more hits, in a programmable pattern, in the first hodoscope H1; ii) a first-level trigger (T1), based on information from the hodoscopes H2 and H3, together with the SAV requirements. Because of the very different production rates, separate triggers for single and multimuon candidates were defined as (T0)·(H2 = 1)·(H3 $\geqslant$ 1)·(SAV) and (T0)·(H2 $\geqslant$ 2)·(H3 $\geqslant$ 1), respectively.

Information from the trigger counters was presented to a cascaded array of 13 programmable logic units [15], each having 8 inputs and 6 outputs (NIM). These units were programmed via the CAMAC dataway, and this permitted each of the six outputs to carry any required logical combination of the eight inputs. This logic was supported by a software system facilitating the generation of different triggers, and automatic re-reading of the memories was run via CAMAC at regular intervals (typically 30 min) to check for corruption of memory patterns and error logging.

The readout system of muon hodoscopes, drift chambers, silicon beam hodoscope, and vertex detector, was based upon the REMUS [16] variation of CAMAC, and the various detector systems each occupied their own branch. The MWPCs of the muon spectrometer and of the vertex detector formed a separate branch which was interfaced to CAMAC rather than to REMUS. A PDP 11/44 was used for data acquisition.

The typical event size was some 3000 16-bit words; the dominant component of this was the 2200 words from the microstrip silicon detectors. The readout time was about 10 ms per event, giving a dead-time of $\sim$ 10% with 20 events per burst and a 2 s spill.

6.3 Exposure and intercalibration

In addition to the main run with the muon trigger, the exposure of a stack included calibration runs with different triggers and particle densities. In the vertical stacks, the central part (22 cm $\times$ 24 cm) was irradiated uniformly at a density of 3000 primaries per mm^2 (Main in fig. 2), and two vertical strips, 1 cm wide, were dedicated to intercalibration runs (fig. 2). Horizontal stacks were exposed twice, in opposite directions, by rotating the frames through 180°. The primary track density, 750 per mm^2 each way, provided a reasonable density of interactions for analysis, but the background with respect to the total flux was halved. Typical beam intensities were 2×10^5 and 5×10^4 particles per burst for vertical and horizontal stacks, respectively.

To link the emulsion reference systems to the rest of the apparatus, an intercalibration procedure, consisting of steps of increasing precision, was applied. This procedure was repeated for

each stack and is described below. For each vertical stack and each face of the horizontal stacks the stage was driven to known positions, where it was kept at rest during a few bursts. In this way, visible (density $> 10^5$ tracks per mm^2) beam 'spots' were formed on the sides of the vertical emulsion sheets or on the thin plates fixed to the horizontal stack holders (figs. 2 and 3). Beam tracks were reconstructed by off-line analysis of the beam hodoscope data, and bidimensional, smoothed contour plots were obtained (fig. 5). By superposition of these plots and the emulsion spots (both scaled to the same dimensions), it was possible to link the reference systems of the MSDs and the emulsions with typical uncertainties of 100 to 200 μm perpendicular to the beam direction.

A further step in the intercalibration procedure consisted of locating, in emulsion, events reconstructed by the VD analysis. In the case of the vertical exposure, special runs were made for each stack in order to collect interactions in four (fig. 3) low-density regions (about 100 primaries per mm^2) using an interaction trigger. These events, once reconstructed and easily located in the emulsion in a relatively large 'fiducial volume', were used to obtain a finer intercalibration by comparing the predicted and found vertex positions. In the case of the horizontal exposures, low-density regions were not needed, and the events to be used for intercalibration purposes were directly selected from the final sample of events. In this way, the link between reference systems was established to less than 50 μm across the beam, as shown in fig. 7.

To define a common origin along the beam, a thin iron plate was mounted on the target mover in a known position with respect to the stacks. It was then exposed to the beam, and a few thousand events were recorded and reconstructed [10]. This procedure located the stacks with respect to the external apparatus within ± 100 μm.

7. OFF-LINE ANALYSIS

The off-line analysis program had a modular design to facilitate running under different conditions and used the HYDRA memory management system. After the decoding of raw data and the alignment of the chambers, the analysis of single triggers proceeded with the reconstruction of muon tracks in the spectrometer. Events with a muon of $p_T \geqslant 0.5$ GeV/c with respect to the beam direction were then analysed in the VD and BH, and the association of the tracks of the muons, before and after the dump, was attempted.

7.1 Decoding of raw data and alignment of the chambers

For each event the data of each piece of equipment were decoded and stored after some preliminary treatments such as pedestal subtraction for the silicon detectors, drift-time determination for the drift chambers, or cluster size analysis for MWPCs. The optimization of T_0 and V_d, the starting time and the drift velocity, was done by fitting a sample of reconstructed tracks, with a method similar to that described in ref. [15], using the T_0 and V_d as parameters to be determined. Geometrical information was also added at this stage.

To obtain the alignment of the detectors, use was made of data collected in dedicated runs during which the magnet was off, and the trigger was chosen so as to select events with beam muons.

7.2 Spectrometer analysis

The analysis started with an independent reconstruction of 'segments' in the chambers downstream from the magnet and 'lines' in those upstream. These were then associated to determine the muon momenta.

A segment was defined as having at least two space points reconstructed in the wire chambers, plus at least one associated hit in the downstream scintillator hodoscope. Space points were reconstructed (independently for each chamber) and associated with hodoscope hits to form the segment. The space lines in the front part of the spectrometer were reconstructed, using three

different algorithms in succession so as to cover the maximum number of geometrical cases, taking into account the large difference in acceptance for the two kinds of detector.

As most of the triggered events contain a single muon in both sets of chambers, its absolute momentum and direction with respect to the beam were computed directly, using the method of Wind [17]. In the case where more tracks were found in either detector, the association between lines and segments was done by comparing, for each possible pair of lines and segments, the slope in the vertical plane and the coordinates, extrapolated to the median plane of the magnet, perpendicular to the beam. All of these quantities are unaffected by the magnetic field. The reconstruction efficiency for a single track turned out to be 85%, whereas the momentum resolution was $\Delta p/p = 6 \times 10^{-4} \times p$ (GeV/c).

7.3 Vertex analysis

The vertex analysis proceeded first to determine single space tracks independently in the BH and in the VD, then to attempt to associate them into a common vertex. In the BH the ambiguities arising from the presence of $\geqslant 2$ tracks were removed by using the less accurate, but valid, transverse coordinates deduced from the VD analysis. Events with either a clear interaction in the VD or $\geqslant 3$ nearly parallel tracks reconstructed (most probably an upstream interaction) were rejected.

In the VD analysis no clustering was assumed, and each fired strip or wire led to a hit, *a priori* considered as part of the track of a particle. The search for tracks was then made separately in the y and z projections, where seven planes were available. A track was defined as having at least one hit in one of the first two silicon detectors, and the fit to a straight line was done using the Chebyshev norm. Space tracks were then obtained by associating those projected tracks found previously, and the u and v projections (six planes each) were used to remove the ambiguities. The parameters of the accepted space tracks [$P(\chi^2) > 0.001$)] were determined by fitting a straight line simultaneously in the four projections. Monte Carlo computation showed that, on the average, 80% of the tracks in projection and 70% of those in space were reconstructed, and the mean number of wrong associations—a strong function of the total multiplicity—was about two for the observed mean multiplicity of twelve. Indeed, as is seen in fig. 8, there is a clear loss for high multiplicities, whereas the small excess for low multiplicities can be almost completely attributed to electron pairs not seen in emulsion at the primary vertex.

The interaction vertex in emulsion was defined as the point for which χ^2 was minimized. However, owing to multiple scattering, secondary interactions, electron pair creation, and decays, some of the tracks observed in the VD did not in reality converge to the primary vertex in emulsion, and the presence of such tracks increased the χ^2 . This was taken into account by iterating the analysis procedure, after having discarded the tracks with the largest impact parameters with respect to the fitted vertex (in units of standard deviations), until a stable solution was found. Finally, an attempt was made to see if any of the 'rejected' tracks (at least three) converged to a common vertex downstream from the primary vertex. A clear correlation was found between events with several rejected tracks and with secondary interactions in emulsion. However, only in very few cases was a secondary vertex found in the predicted position, and in no case was a decay topology detected in this manner.

7.4 Muon association

Since the muons were detected after a dump (section 3) equivalent to 110 radiation lengths (or 570 in the central tungsten core), the energy loss and the multiple scattering are not negligible and seriously affect both the p and p_T determined in the spectrometer. On the other hand, as the muon track was also 'seen' before entering the dump, the association between a track in the vertex detector and that reconstructed in the spectrometer would render negligible the error on p_T and reduce the

background. The corrected momentum (p_{corr}) was obtained by adding the measured one to that corresponding to the energy loss (including bremsstrahlung) in the dump. A corrected value θ_{corr} of the emission angle of the muon (fig. 9) was obtained by the combination of θ_2 (the measured angle after the dump) and θ_1 (an 'inferred' production angle), which minimizes the error due to multiple scattering. According to the method shown in ref. [18], θ_{corr} is given by

$$\theta_{corr} = w\theta_1 + (1 - w)\theta_2$$

and

$$\sigma_{\theta_{corr}} = (1 - w)^{1/2}\, \sigma_{\theta_2} ,$$

where

$$w = [1 + l^2/(12x_0^2)]^{-1} ;$$

σ_{θ_2} is the error on θ_2 expected from multiple scattering in the dump, and $\sigma_{\theta_{corr}}$ is the error on θ_{corr}.

The production point was assumed to be the centre of the emulsion stack along the nominal beam. As expected, in our conditions ($l \simeq x_0$) the error on θ_{corr} is more than three times smaller than that on θ_2, and this allows the association to be made much more efficiently.

Figure 10, which shows the distribution of the quantity $R = |\theta_2 - \theta_{corr}|/\sigma_{\theta_2}$, indicates that the errors are evaluated correctly. A long tail for high values of R, only apparent when the p_T cut is applied, is mainly due to muons in the beam halo which therefore, despite their usually high momentum, seem to have suffered a large scattering when constrained to originate from the target. These events were removed by requiring $R \leqslant 4$, without an appreciable loss of genuine events.

Figure 11 shows, for a sample of events selected with $p_T \geqslant 1$ GeV/c and $R \leqslant 4$, the distribution of the quantity $S = |\theta_{corr} - \theta_{VD}|\sigma_{\theta_{corr}}$, where θ_{VD} is the angle of a track in the vertex detector. Here all the space tracks of each event were considered, whereas the shaded area represents events in which only the VD track with direction closest to θ_{corr} was kept. It is easily seen that there is a clear signal for small values of S, well above the combinatorial background. For $S < 3$, most of the associations are unambiguous, a multiple association being possible only in about 10% of the cases. Events where the track closest to the muon track was found to have $S > 4$ (25% of the cases) were considered as not being associated and were rejected; the reason was often an inefficiency in the reconstruction of space tracks in the VD (see also subsection 8.3).

7.5 J/ψ signal

An overall check on the quality of the muon reconstruction and association procedures was performed by analysing events with opposite-sign dimuons and trying to establish a J/ψ signal. Events were selected in which the transverse momentum of both muons with respect to the beam direction was $\geqslant 1.0$ GeV/c. The invariant mass of the pair was then computed (fig. 12) by using a) spectrometer parameters and absolute momenta, corrected for energy loss in the dump, b) the corrected angles θ_{corr}, which take into account both multiple scattering and the production point, and finally c) the angles given by the VD analysis, where a single unambiguous track was associated with each muon. It is seen that whilst a peak around the J/ψ mass value is observed in all three distributions, its width and central value are greatly improved when there is a good association with the VD. The much more accurate angles measured there and the possibility of rejecting a larger fraction of the asymmetrical background—already substantially reduced at low masses by the p_T

cut—are the main contributions to the improvement. The fact that the value of the J/ψ mass is well reproduced shows that no large residual systematic error existed.

8. SEARCH IN EMULSION

8.1 Sample definition

Before searching for the events in emulsion, the sample was further 'cleaned' by selecting events which were reasonably well reconstructed and had good muon association. Events with a single reconstructed muon—the bulk of our data—were selected if the corrected momentum, transverse to the direction of the beam, was larger than 1.0 GeV/c (0.6 GeV/c for a subsample). Events with two opposite-sign muons were treated as single-muon events by neglecting the lower-p_T muon, but events with two like-sign muons or with more than two muons were retained, regardless of their p_T value.

The next step was the selection of events with a good muon association between the spectrometer and the VD ($R \leqslant 4$ and $S \leqslant 4$: subsection 7.4), including cases where there was ambiguity between two or more reconstructed tracks.

Finally, quality and fiducial volume cuts were applied, by rejecting events

- with less than four space tracks accepted in the standard VD reconstruction procedure;
- with the 'beam' track displaced by more than 200 μm from the primary vertex reconstructed by the VD alone;
- situated within 2 mm of the edge of plates of the horizontal stacks ($\sim$ 14% loss), or in the three most downstream sheets (which were used only for measurement purposes and for the decay search), and within 1 mm of the edge of the remaining modules of the vertical stacks ($\sim$ 25% loss).

8.2 Event location

The selected events were searched for in emulsion by means of a volume scan around the predicted point, after the intercalibration procedure (section 6) had successfully located the first event. Typical 'fiducial volumes' were defined as ± 200 μm across and $\pm$(1.5 to 3) mm along the beam, depending on the event topology and position. This volume contained very few primary or secondary interactions, and usually a quick comparison of the forward-emitted minimum ionization prongs with the predicted features of the searched-for event was sufficient to discriminate between candidates and background.

As can be seen in fig. 13, where the distribution of differences between predicted and measured coordinates along the beam direction are shown, the primary vertex of predicted events was found regardless of the presence of decay topologies or of secondary interactions. In these latter cases, in fact, the Δx distribution is $\sim$ 15% wider, but no shift of the central value is observed. The finding efficiency of events was, on the average, above 80%, the sources of loss being either real inefficiency or incorrect scanning volumes. The first kind of loss was made up of both genuine scanning inefficiency and of poorly reconstructed events, where too many wrong associations in the building up of space tracks rendered the searched-for event very different from the actual one. The second kind of loss arose from incorrect rv nstruction of the primary vertex, in cases where too many 'wrong' tracks (scattered, emerging from undetected secondary interactions, etc.) were used and not subsequently rejected. As the overall efficiency was reasonably high and the sources of loss were many, being no higher for 'interesting' events than for 'normal' ones, no attempt was made to increase the efficiency further. Figure 14 shows the overall location efficiency as a function of the coordinates of the production point. The decrease of efficiency with increasing thickness of the residual target was expected, owing to the increasing importance of effects such as scattering, secondary interactions, and γ-ray conversions; events containing decay topologies show the same trend as the whole sample.

8.3 Measurements

The angles of the minimum-ionization prongs emitted within ~ 200 mrad of the beam direction were measured for candidate interactions found in emulsion, and were compared with the predicted space tracks or with tracks reconstructed in one or more projections and not associated in the standard reconstruction procedure. These measurements, usually to better than 1 to 2 mrad in both azimuth and dip, were accurate enough to match the observed tracks with the predicted ones, almost without ambiguity. The event features observed at the interaction vertex in emulsion agree well, on the average, with those predicted from the VD analysis, but predictions were generally found to be less reliable towards the limits of the VD acceptance or when the number of tracks per event increased. Figure 15 shows the average efficiency in associating emulsion and VD space tracks as a function of the emission angle; it is seen that the VD efficiency is nearly constant (but depends on the multiplicity, fig. 8) for angles up to 100 mrad, within which > 75% of the charged particles from the interactions and > 95% of the triggered muons are confined.

The scanning and measuring power provided by the Collaboration was enhanced by the use of automated microscope stages and computer-aided data-acquisition systems, and by local software and graphics facilities. Depending on the kind of emulsion analysed and on the instruments available for the analysis, the actual procedures adopted by different laboratories were different for both scanning and measurement. However, all laboratories followed the guidelines listed above, and the results obtained so far are quite homogeneous and comparable, except those which depend on objective differences, such as the target thickness.

8.4 Search for decays

In fig. 16 the distributions of the distance of closest approach to the predicted vertex are shown separately for tracks of muons and for other space tracks found in emulsion which converge to the primary vertex or which belong to a decay topology. The various sources of error and of ambiguity — also linked to the thickness of the target — precluded any possibility of selecting events most likely to contain decay topologies. Therefore, a search for decays had to start in the emulsion.

As the muons which caused the event to be selected are of interest only if they come from decays of unstable particles, the search was only performed for events having at the primary vertex no track with angles compatible with those predicted for any of the muons within $\Delta\theta$ (mrad) $= 3 + 0.05 \times \theta$ (mrad). About 10% of the events fell into this class. The others were not analysed any further, apart from a careful inspection close to the vertex. The search for decays was conducted in different ways for neutral and charged topologies, and also with different techniques in the vertical and horizontal emulsions. As a common guideline, the first goal was to search for the decay from which the muon was emitted. Of course, all decays due to charged particles and a fraction of those due to neutral ones were already detected if they had occurred within the range used for measuring the forward prongs emerging from an interaction.

Decays due to charged particles were searched for by means of an along-the-track scanning technique starting, in each case, from the primary vertex. This was applied to all the forward-emitted (< 150 mrad) tracks not associated with tracks seen in the VD and to a sample of those associated. Each track was followed to the exit edge of the stack for the vertical sheets or, usually, to the exit point of the pellicle for the horizontal ones.

Decays due to neutral particles were usually sought by means of a volume scan downstream from the primary interaction in both kinds of emulsion. The minimum volume in which the search was performed was that of a cylinder of radius 200 μm (around the primary vertex) and length 3 mm, but the length was increased to 7 mm, if possible, in most cases. As a volume scan is known to have a lower efficiency, the search for neutral — and sometimes for charged — decay topologies was also carried out using the method of picking up tracks with given angles crossing a fiducial surface

(normally close to the front end of the stack), and following them back towards the primary interaction, or up to the point where a decay topology was found. Angles and coordinates were those predicted by the VD analysis. Neutral-decay topologies were considered as associated with the event if at least one prong matched a VD track unambiguously.

The question of further study of 'interesting' events in which decay topologies were in fact found (or were not found) was based on the merits of each individual case, and depended on the distance from the primary vertex to the exit edge of the stack, on the residual tracks reconstructed in the VD but not found in emulsion, etc. It was observed that more than 50% of cases where the muon was 'missing' at the primary vertex indeed showed at least one decay topology, and in most cases the muon was associated with one of them. In some cases the muon was seen to originate from a secondary interaction, which was recognized as such, either by the presence of 'heavy' (evaporation) prongs or because the number of charged particles was not consistent with a decay topology.

9. THE 1984 RUN

In the 1984 run the experimental set-up was modified (section 1) by replacing the dump by the WA78 uranium-iron hadron calorimeter. The target and vertex detector were positioned ~ 1.4 m further upstream, resulting in a smaller acceptance for muons, but the information provided by the calorimeter on the energy, and in particular on the 'missing' energy E^{miss}, for events containing otherwise undetectable neutrinos, permitted a more stringent event selection to be made. Only minor changes were made to the rest of the apparatus: the silicon beam counters (BC: subsection 6.1) were removed so as to reduce the background due to upstream interactions and the 'event' signal was taken from the interaction counters IC; the SAV was replaced by a more versatile 'diaphragm' counter; a veto wall was inserted ~ 2 m upstream of the target. The beam characteristics were similar, but the spill-time was increased to 2.6 s and the cycle length to 14.4 s. Because of the relatively low trigger rate during the exposures, no on-line selection on E^{miss} was required, and the off-line analysis showed the energy resolution to be $\sigma_E/E = 4.7\%$ for interactions located in the emulsions, situated ~ 1 m upstream of the calorimeter.

Figure 17 shows the distribution of E^{miss} for those events which, selected according to a muon p_T cut of $\geqslant 1$ GeV/c, were found in emulsion, and in which the muon was either seen or not seen at the primary vertex (in these latter cases the search for decay topologies is being carried out). Although this analysis is, as yet, incomplete, it can easily be seen from a comparison of the two histograms that a cut on E^{miss} (with $p_T \geqslant 1$ GeV/c) improves the efficiency for selecting these potentially 'interesting' events. As an example, 52% of the events with the muon seen at the primary vertex have $E^{miss} > 0$, whereas the fraction increases to 63% for those where the muon is not seen.

On the basis of these and similar results, the following selection criteria were used for data of the 1984 run:

a) $0.6 \leqslant p_T < 1.0$ GeV/c, $\quad p_T + E^{miss}\,(\text{GeV})/80 \geqslant 1.5$,

b) $p_T \geqslant 1.0$ GeV/c, $\quad E^{miss} \geqslant 0$.

10. ACCEPTANCE AND SENSITIVITY

10.1 Acceptance

Muon acceptances were calculated using a heavy-flavour (charm, beauty) production mechanism:

$$\frac{d^2\sigma}{dx dp_T^2} = (1 - |x|)^3 \exp(-1.1 p_T^2) \qquad (p_T \text{ in GeV/c}) .$$

The assumed decay modes for beauty and charm were $B \rightarrow \mu + \nu + D$ and $D \rightarrow \mu + \nu + K$,

respectively; the muons generated in these decays were tracked through the apparatus, and then reconstructed using the standard analysis program and taking into account the various efficiencies. Acceptances were calculated as functions of the minimum muon p_T and the emission angle θ with respect to the beam direction for both 1983 and 1984 experimental configurations. Figures 18 and 19 show the acceptance as a function of θ for events containing a pair of beauty or charmed particles, and in which only one muon is generated in the decay processes. The effects of p_T cuts are shown, and it is seen that, for the beauty sample, once the constraint of $p_T \geqslant 1$ GeV/c is applied, a SAV (of $\theta < 20$ to 30 mrad) does not affect the acceptance too much. This fact was used to reduce the on-line trigger rate. The same is true for the charm signal, but there the $p_T \geqslant 1$ GeV/c cut reduces the acceptance to less than 10% of that for beauty owing to the fact that, for the smaller charm mass, the production angle is effectively constrained more strongly than the decay angle.

Multimuon decays have been treated in the same way. The aceptance for the case of at least one detected muon is about twice that in the previous case, but of course its contribution to the overall signal is about a factor of 10 smaller, owing to the semileptonic decay rate.

10.2 Sensitivity

It is beyond the scope of this experiment to determine the production cross-sections for beauty and charm, but an order-of-magnitude estimate can be made from the sensitivity and the number of observed events. The sensitivity S_n, expressed as the number of events per unit cross-section, can be factorized as

$$S_n = \frac{N_{int}}{\sigma_\pi} \times \frac{A^x}{A^{2/3}} \times P(\geqslant 1\,\mu) \times \alpha \times \epsilon \times \varrho \times \phi \times \delta,$$

where N_{int} is the number of primary interactions produced in emulsion within the fiducial volume;

σ_π is the pion inelastic cross-section ($\sim$ 20 mb);

x is the exponent of the A-dependence of the process considered;

$P(\geqslant 1\,\mu)$ is the probability that at least one muon is produced from the decay of a pair of particles;

α is the acceptance of the apparatus;

ϵ is the efficiency of the apparatus (including dead-time);

ϱ is the reconstruction efficiency [muon(s), beam, vertex];

ϕ is the ratio of found to predicted events;

δ is the efficiency in detecting the decays in emulsion (including geometrical losses).

As a rough estimate, the sensitivity of the WA75 experiment for beauty will be in the range from 0.3 to 0.5 events per nb/N after completion of the scanning, assuming $x = 1$, $P(\geqslant 1\,\mu) = 0.24$, $\epsilon = 0.8$, $\varrho = 0.5$, $\phi = 0.8$, and $\delta = 0.5$; it includes the acceptances for the different experimental configurations and selection criteria used. Of course, the final analysis will take into account the dependence of δ on the mean lifetime and will estimate the various factors with higher accuracy. It is seen, however, that the single event already found [3] gives an order-of-magnitude estimate of the production cross-section in agreement with the result of WA78 [19], i.e. $\sigma = (2.0 \pm 0.3 \pm 0.9)$ nb/N for a linear A-dependence. If the same values of all the factors (except α) are used for charm production, the sensitivity of the experiment will be in the range from 20 to 50 events per μb/N for a linear A-dependence of the cross-section. The present status of the analysis—about 60% of the material fully analysed and $\sim$ 200 events found with decay topologies consistent with charmed-particle decays [20]—would indicate a charm production cross-section of the order of 10–20 μb/N.

Acknowledgements

It is a pleasure to thank the many people who helped us through the various stages of the experiment, and without whose contribution any appreciable results would not have been obtained. Among them we wish to mention M. Carchia, C. Casey, P. Dechelette, R. Diotallevi, F. Fiorello, D. French, K. Itoh, L. Liberti, M. Renevey, F. Rodriguez and H. Watson. The continuous assistance of Michelle Mazerand was inestimable.

We gratefully acknowledge the support of the CERN Management, of the DD, EF, EP, and SPS Divisions, and of the Omega and Emulsion Groups. We received valuable help from the Rutherford Appleton and KEK Laboratories, as well as from the Pisa NA1 and Genova WA7 Groups. Support from the Mitsubishi Foundation, from the Japan Society for the Promotion of Science, and from the Ministry of Education, Science and Culture in Japan, is greatly appreciated.

REFERENCES

[1] J.P. Albanese et al., proposal CERN/SPSC/81-69, P166 (1981).

[2] Particle Data Group, Phys. Lett. **170B** (1986).

[3] J.P. Albanese et al., Phys. Lett. **158B** (1985) 186.

[4] S. Aoki et al., Phys. Lett. **187B** (1987) 185.

[5] M.G. Catanesi et al., Nucl. Instrum. Methods **A253** (1987) 222.

[6] R. Arnold et al., Phys. Lett. **186B** (1987) 435.

[7] K. Hoshino and G. Rosa, Nucl. Tracks and Rad. Meas. **12** (1986) 477.

[8] S. Aoki et al., Nucl. Tracks and Rad. Meas. **12** (1986) 249.

[9] G. Romano, report CERN 85-18 (1985).

[10] R. Alberganti et al., Nucl. Instrum. Methods **A248** (1986) 337.

[11] J. Kemmer, Nucl. Instrum. Methods **169** (1980) 499.

[12] M. Bozzo et al., Nucl. Instrum. Methods **178** (1980) 77.

[13] L. Van Koningsveld et al., Internal note on CERN-EP electronics instrument 247 (19.12.1977) (unpublished).

[14] J.B. Lindsay et al., Nucl. Instrum. Methods **156** (1978) 329.

[15] A. Fucci et al., Nucl. Instrum. Methods **147** (1977) 587.

[16] C. Jacobs and L. McCulloch, CERN CAMAC Notes 63 and 64 (1976).

[17] H. Wind, Nucl. Instrum. Methods **115** (1974) 431.

[18] J.G. Branson et al., Phys. Rev. Lett. **38** (1977) 1334, and references quoted therein.

[19] M.G. Catanesi et al., Phys. Lett. **187B** (1987) 431 and **202B** (1988) 453.

[20] S. Aoki et al., preprint CERN-EP/88-52 (1988), to be published in Phys. Lett. B.

Table 1

Geometrical characteristics of microstrip silicon detectors

Detector	No. of planes	No. of strips	Dimensions (mm)	Pitch (μm)	Strip directions (z = 0°) (deg.)
BH	1–6	200	30 × 10	50	90, 0, 90, 0, 90, 0
VD	7, 8	400	20 × 20	50	0, 90
VD	9, 10	400	40 × 40	100	0, 90
VD	11–14	200	40 × 40	200	0, 45, 90, −45
VD	15, 16	400	20 × 20	50	45, −45

Table 2

Spectrometer chambers characteristics

Chamber	No. of planes	Dimensions (cm)	Wire spacing (mm)	Wire directions (z = 0°) (deg.)
MWPC 1	4	32 × 32	1	90, 0, 45, 135
MWPC 2	4			
MWPC 3	4			
DC 1	3	131 × 91	48	0, 90, 0
DC 2	2	192 × 37	50	10.14, 90
DC 3	2			−10.14, 90
DC 4	2			10.14, 90
MWPC 4	4	232 × 232	2	0, −28.07, 90, 28.07
MWPC 5	4			
MWPC 6	4			

Figure captions

Fig. 1 Layout of the WA75 experiment (set-up used in the 1983 exposures).

Fig. 2 Composition of a 'vertical' stack built up with 25 double-coated sheets. A sketch of the exposure scheme is shown.

Fig. 3 Sketch of a 'horizontal' stack, built up with approx. 60 stripped emulsion pellicles, and relative positions of beam hodoscope and vertex detector.

Fig. 4 The target mover.

Fig. 5 Shape of the beam cross-section: smoothed contours at 70%, 40%, and 10% of maximum density (+) were obtained from the beam-hodoscope analysis.

Fig. 6 Schematic side view of the beam hodoscope and of the first part of the vertex detector surrounding the target (mounted on the target mover TM); BC and IC are beam and interaction counters, described in section 6.

Fig. 7 Distributions of differences between predicted and measured coordinates of primary vertices across the beam.

Fig. 8 Correlation between the average number, per event, of reconstructed space tracks ($\langle n \rangle_{VD}$) and the number of tracks found in emulsion (n_{em}) within the acceptance of the vertex detector.

Fig. 9 Distances and angles used to determine the corrected emission angle of the muon affected by the minimum error due to multiple scattering.

Fig. 10 Distribution of $R = |\theta_2 - \theta_{corr}|/\sigma_{\theta_2}$ for a sample of events reconstructed in the spectrometer.

Fig. 11 Distribution of $S = |\theta_{corr} - \theta_{VD}|/\sigma_{\theta_{corr}}$ for events with $R \leqslant 4$. The shaded area represents data where, in each event, only the track with direction closest to θ_{corr} was considered.

Fig. 12 Invariant mass of $\mu^+\mu^-$ pairs (both muons with $p_T \geqslant 1.0$ GeV/c) using: a) uncorrected spectrometer angles; b) corrected spectrometer angles; c) VD angles when an unambiguous association was possible.

Fig. 13 Distribution of differences between predicted and measured coordinates of primary vertices along the beam direction. Events containing decay topologies (dashed line; histograms normalized) are more dispersed — by about 15% — but not systematically shifted.

Fig. 14 Overall location efficiency (found/searched-for events) as a function of the residual thickness (x) of the target.

Fig. 15 Fraction of emulsion tracks matched with reconstructed space tracks in the VD as a function of the emission angle. The dashed line represents the fraction of measured emulsion tracks up to an angle θ.

Fig. 16 Normalized distributions of the distance of closest approach to the predicted vertex for the following categories of tracks seen in emulsion: hadrons to (a) primary and (b) secondary vertices; muons to (c) primary and (d) secondary vertices.

Fig. 17 Distribution of missing energy for events with $p_T \geqslant 1$ GeV/c. The dashed line represents events where, according to a preliminary analysis, the muon is not seen at the primary vertex.

Fig. 18 Acceptance of the WA75 apparatus for muons from beauty-particle decays as a function of the angle θ with respect to the beam direction. Curves are for the various selection criteria.

Fig. 19 Acceptances as in Fig. 18 for muons from charmed-particle decays.

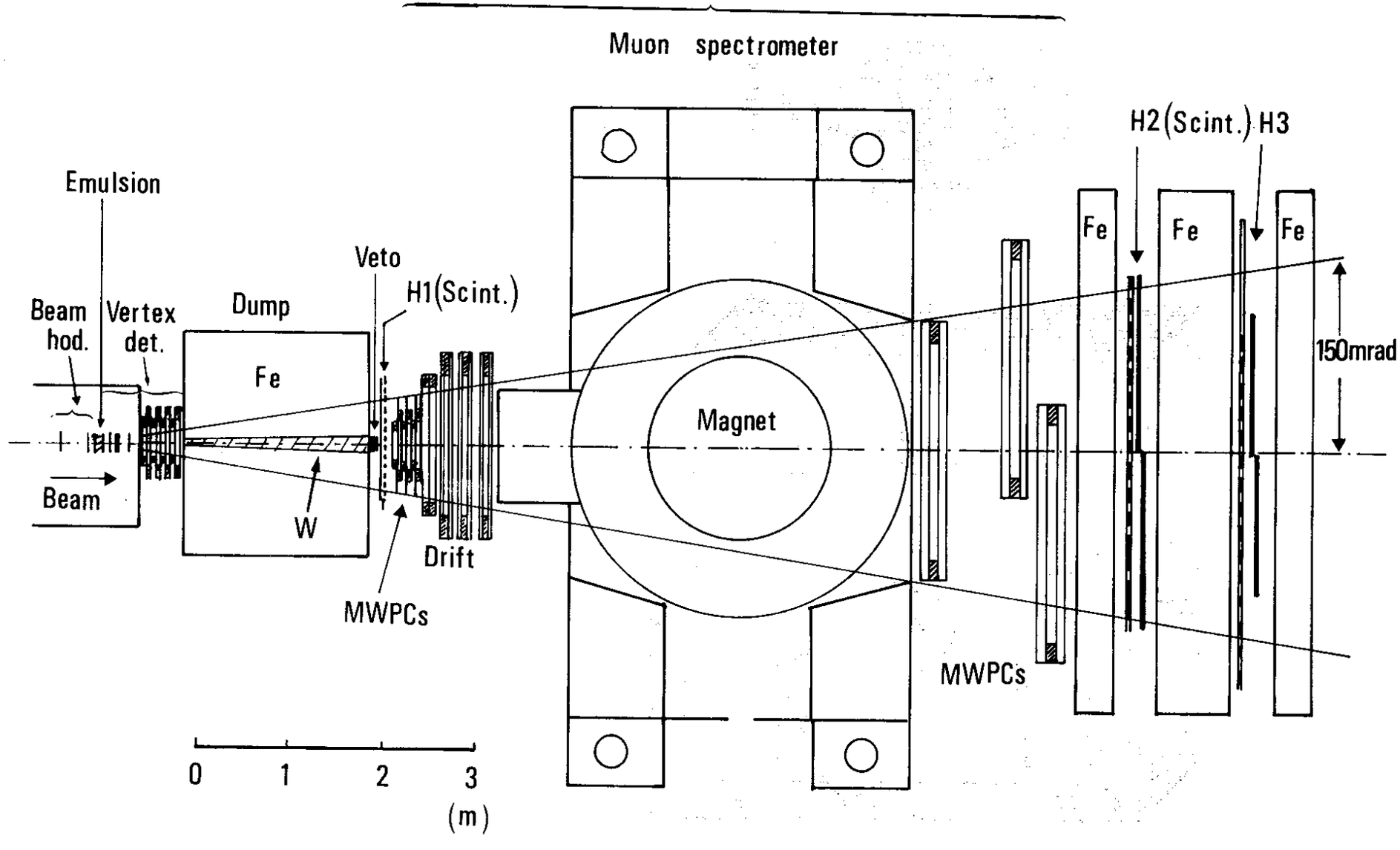
Muon spectrometer
Emulsion
Beam hod.
Vertex det.
Dump
Fe
Veto
H1(Scint.)
Beam
W
Drift
MWPCs
Magnet
H2(Scint.)
H3
Fe
Fe
Fe
150mrad
MWPCs
0
1
2
3
(m)

Fig. 1

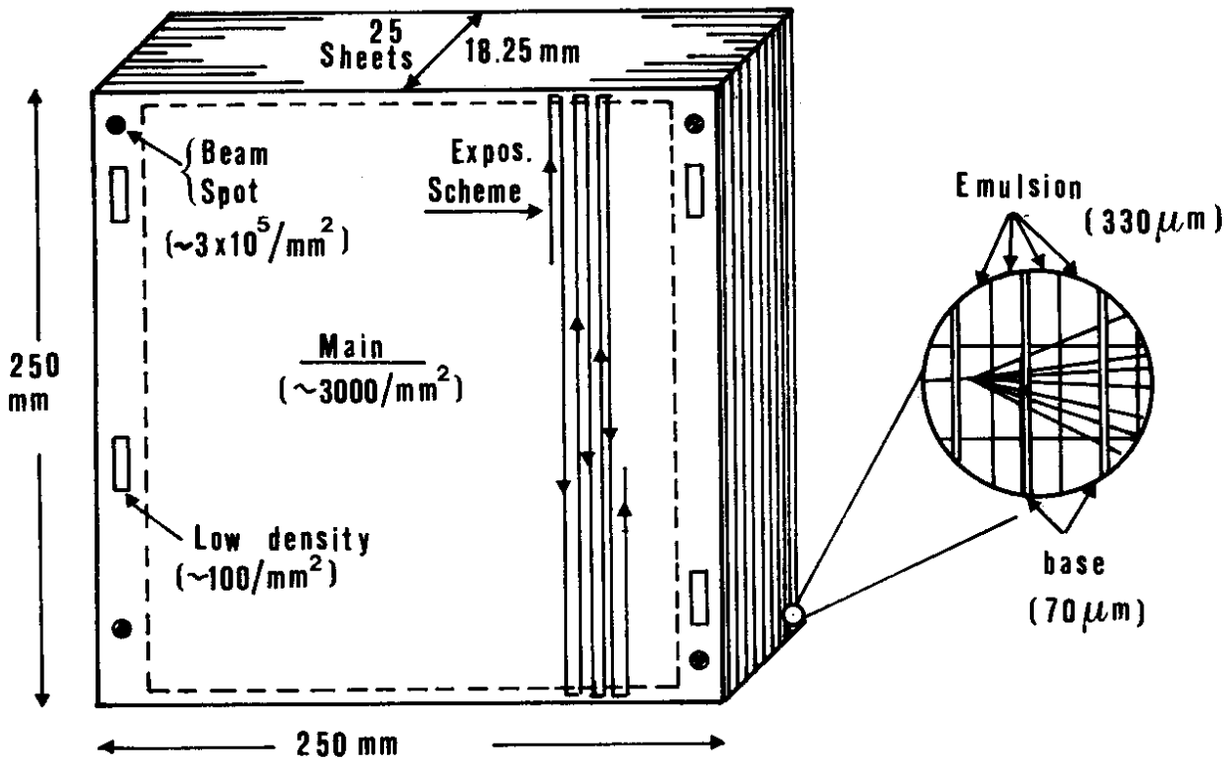
25
Sheets
18.25 mm
Beam
Spot
(~3x10^5/mm^2)
Expos.
Scheme
Main
(~3000/mm^2)
Low density
(~100/mm^2)
250
mm
250 mm
Emulsion
(330μm)
base
(70μm)

Fig. 2

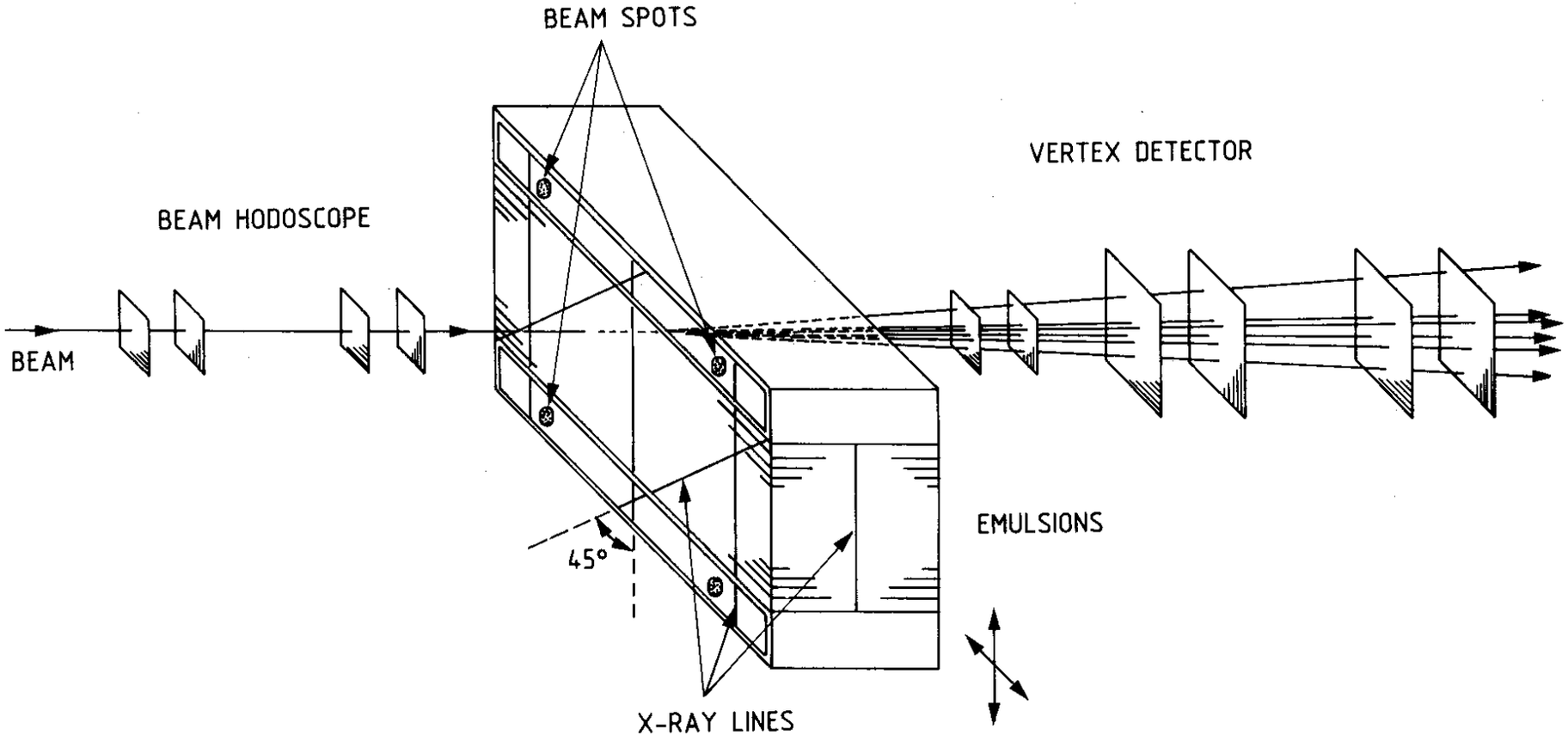
BEAM SPOTS
VERTEX DETECTOR
BEAM HODOSCOPE
BEAM
EMULSIONS
45°
X-RAY LINES

Fig. 3

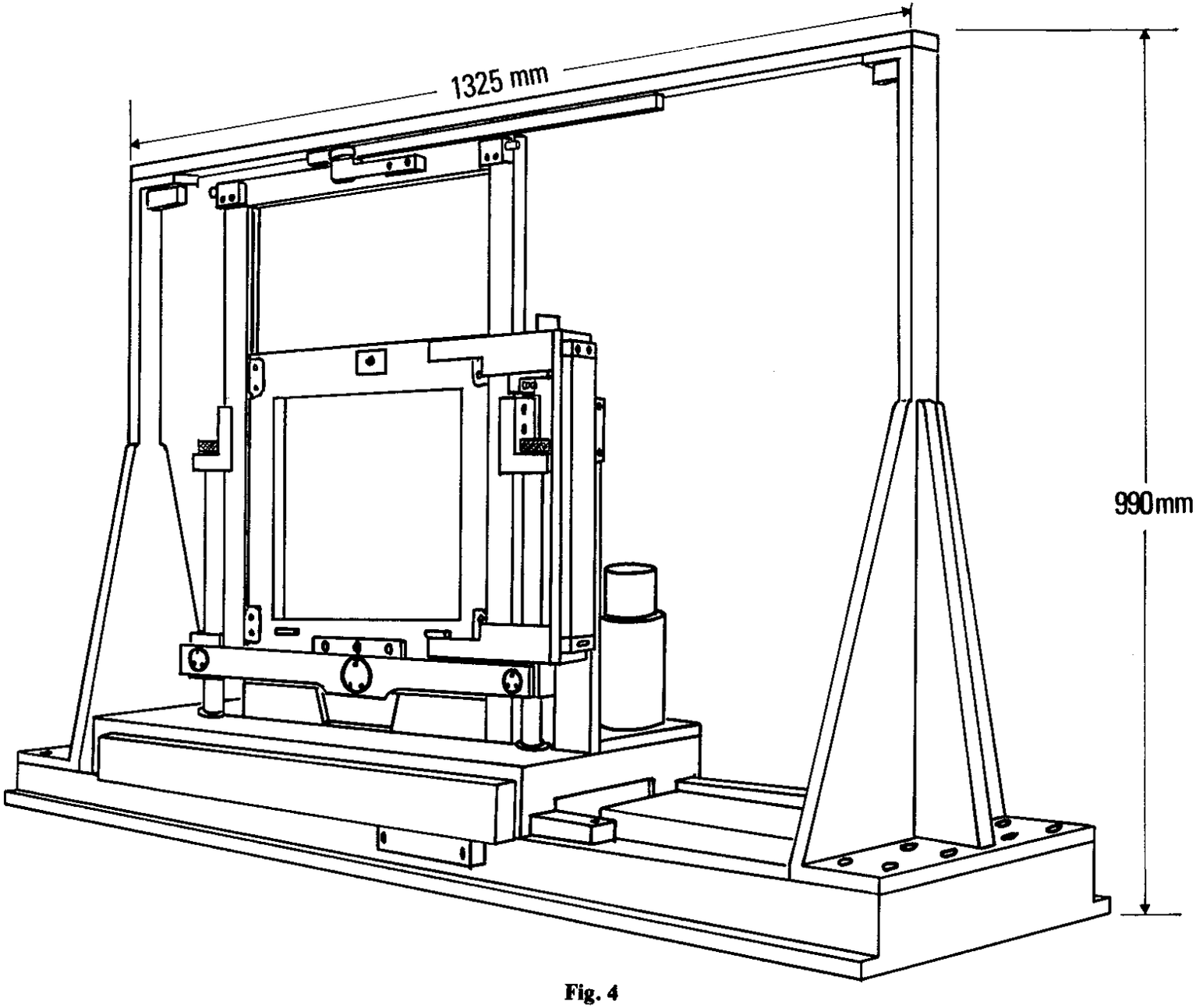

Fig. 4

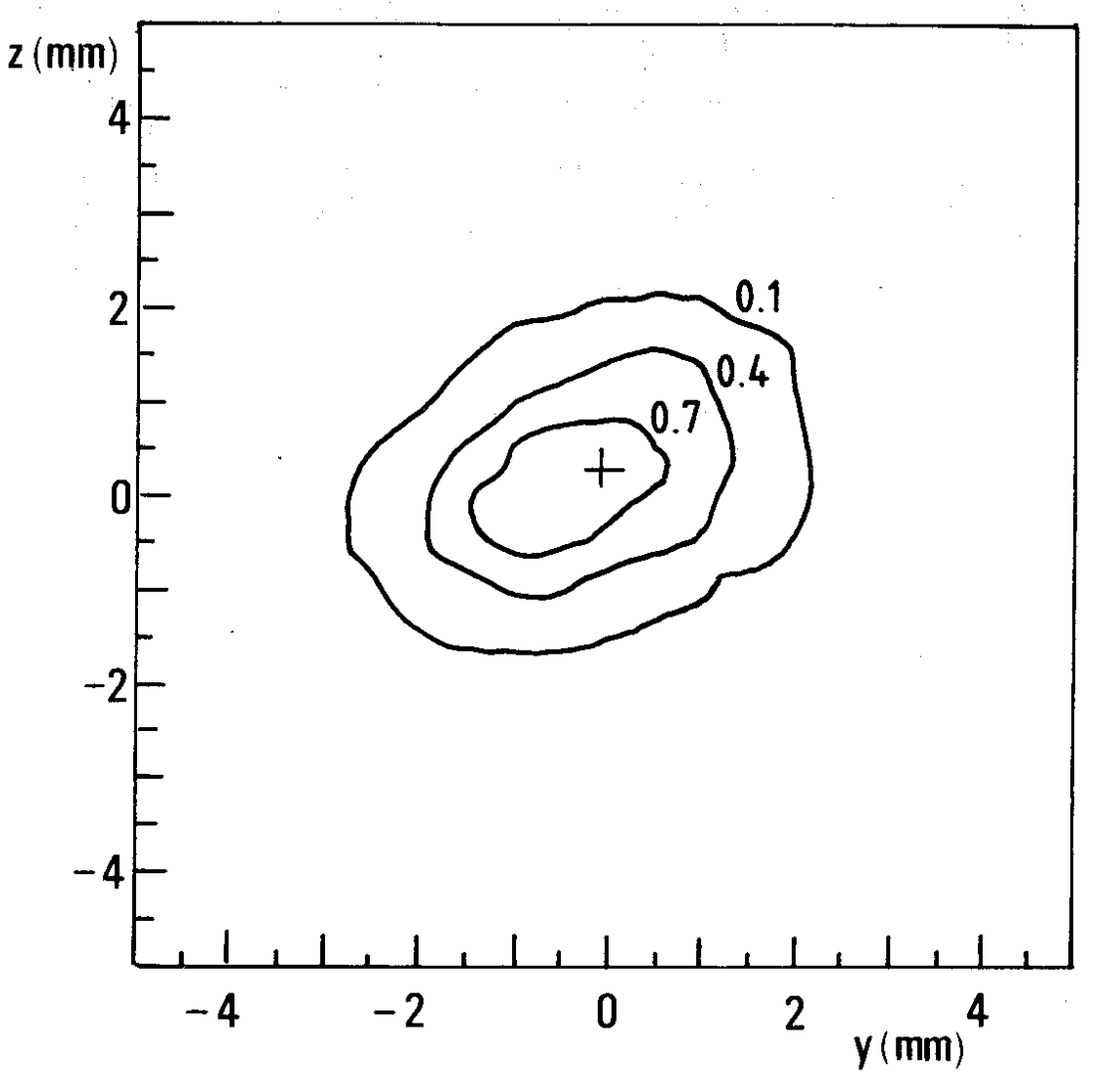

Fig. 5

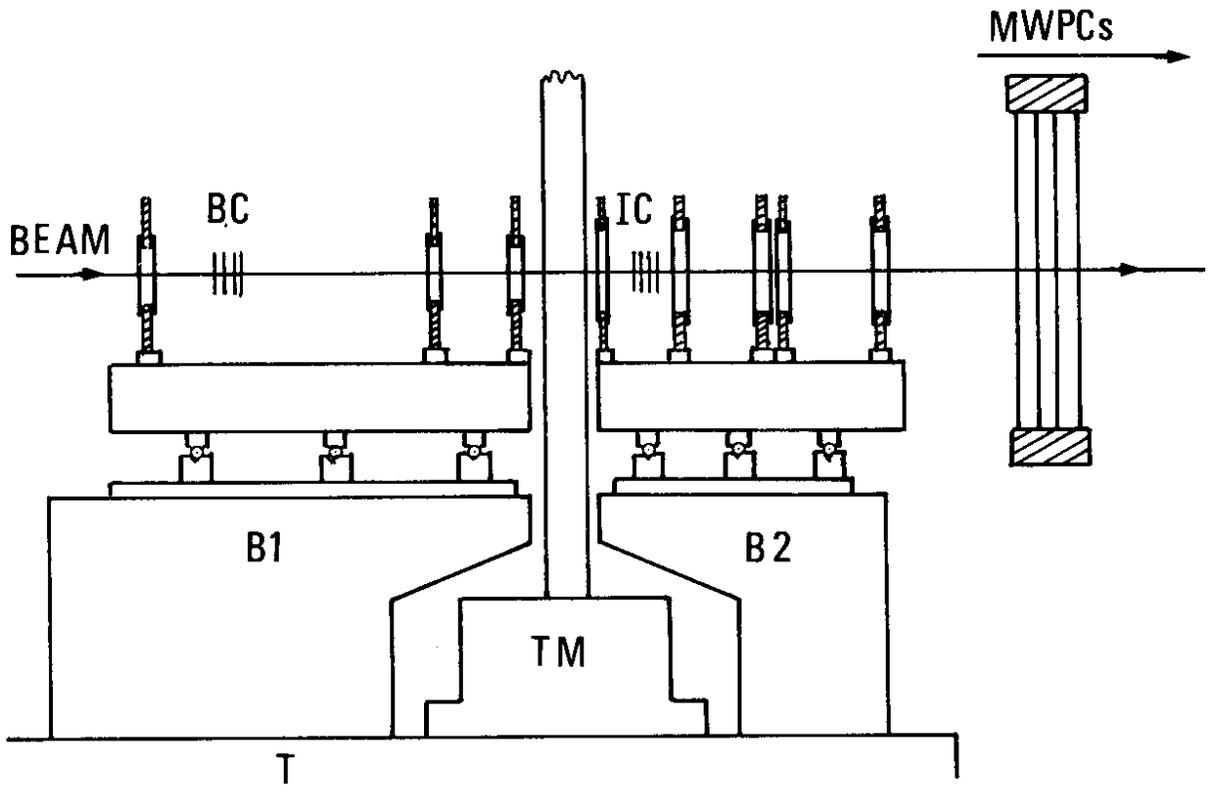
MWPCs
BEAM
BC
IC
B1
B2
TM
T

Fig. 6

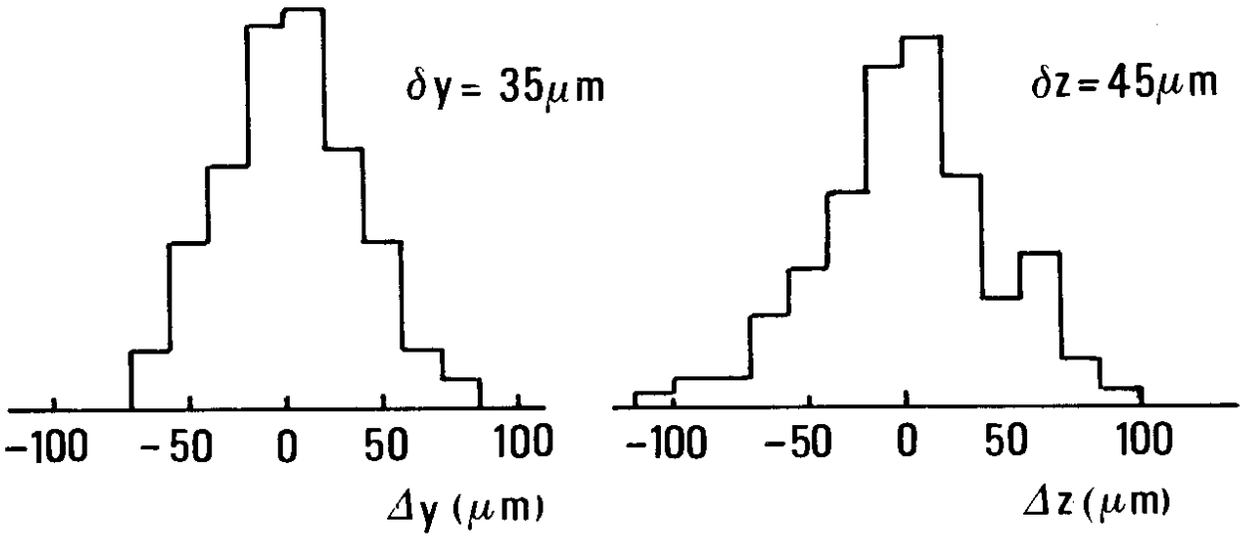
δy = 35μm
δz = 45μm
-100
-50
0
50
100
Δy (μm)
-100
-50
0
50
100
Δz (μm)

Fig. 7

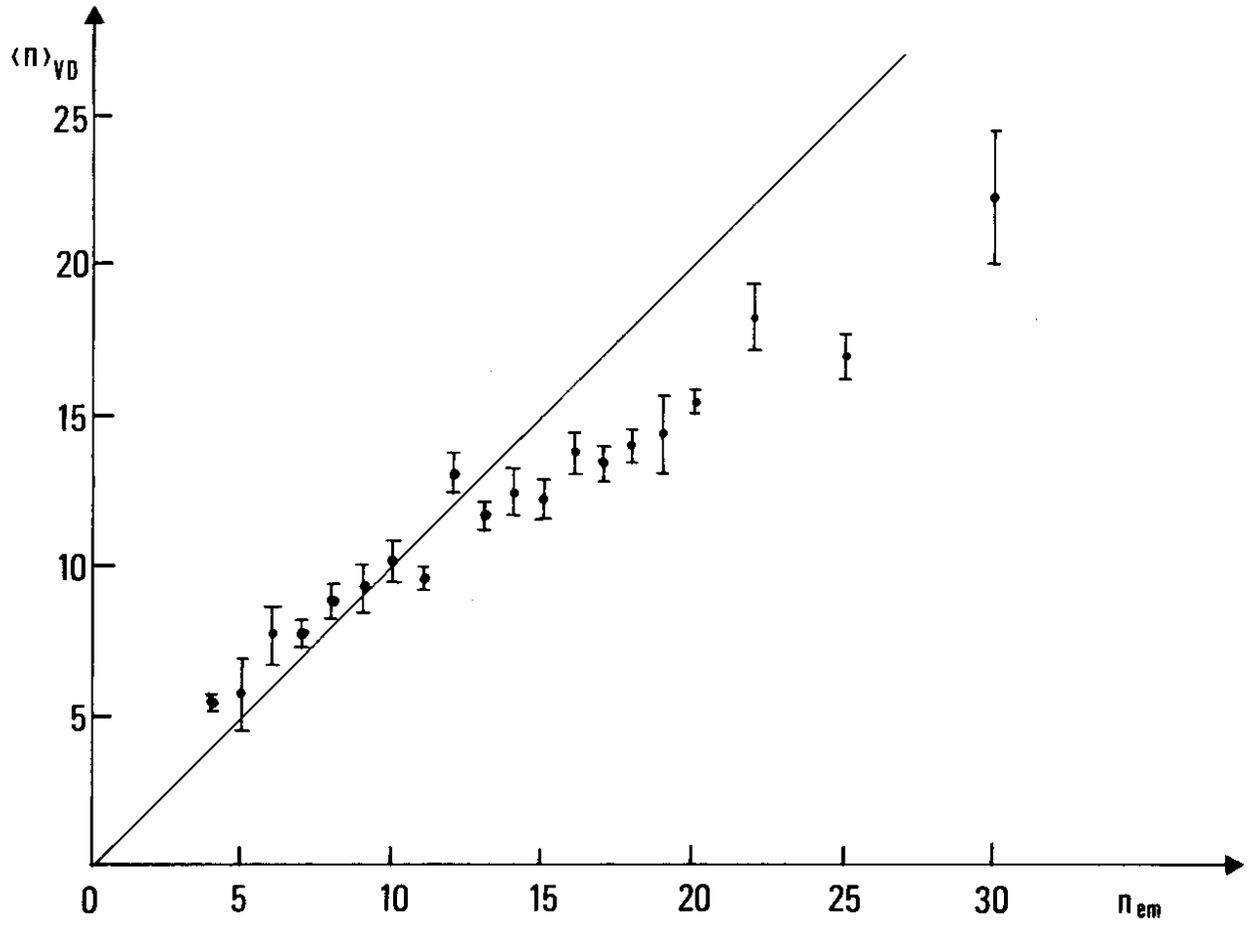

Fig. 8

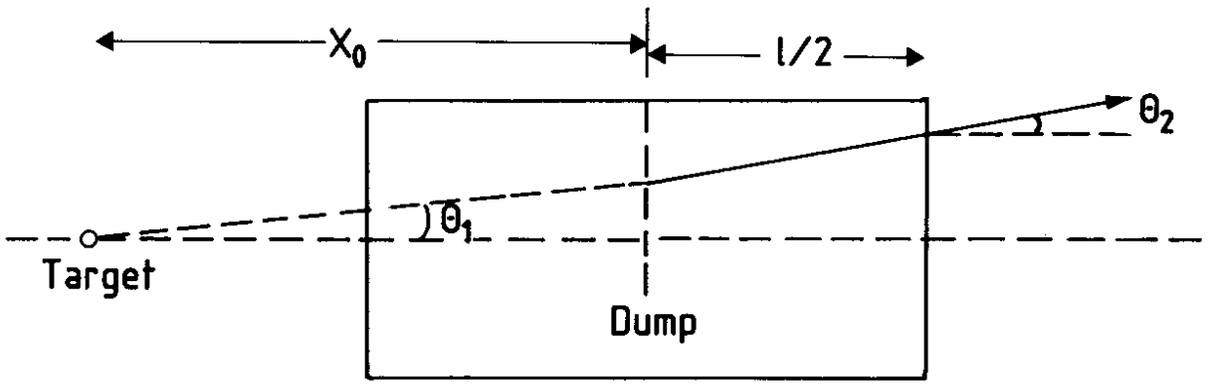

Fig. 9

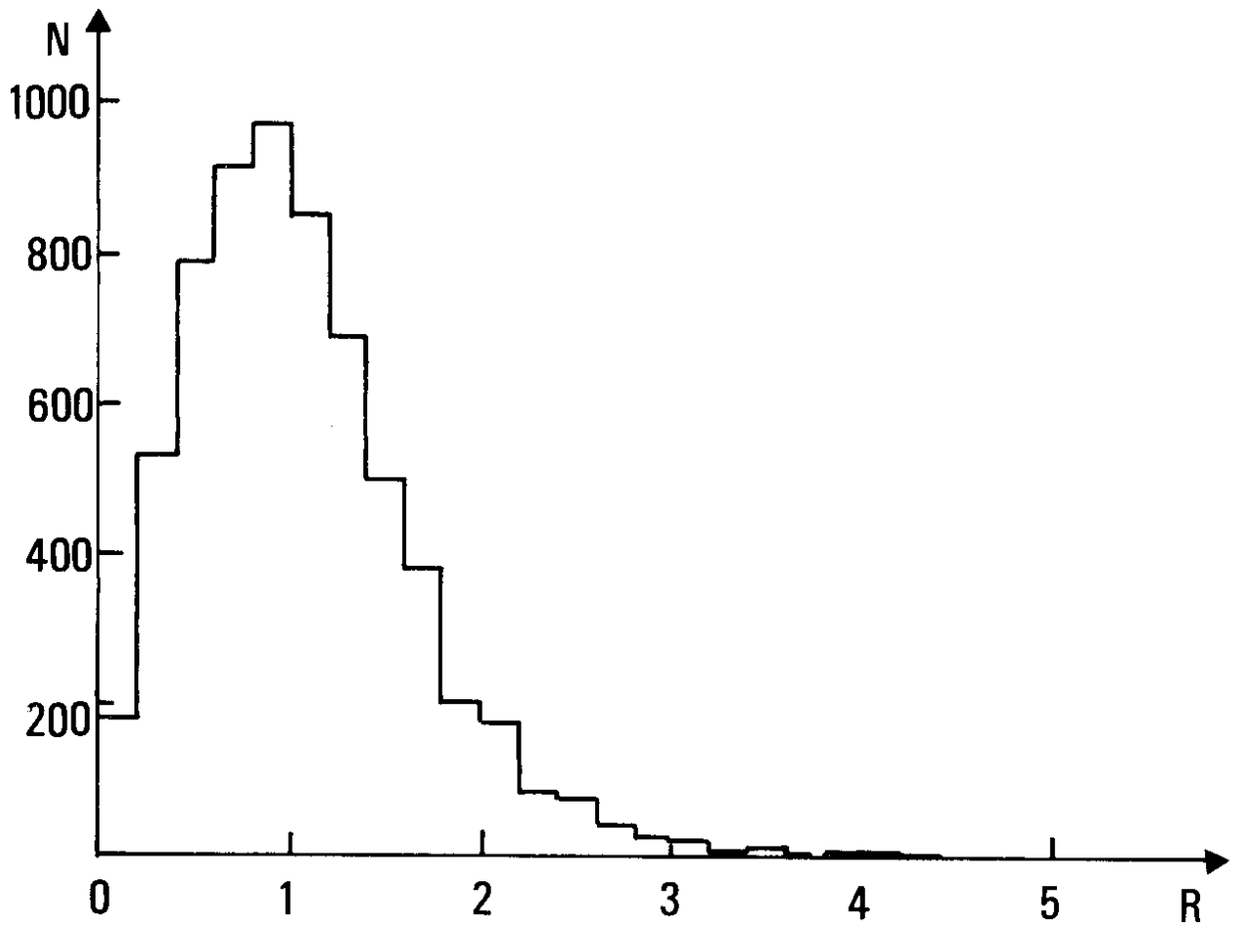

Fig. 10

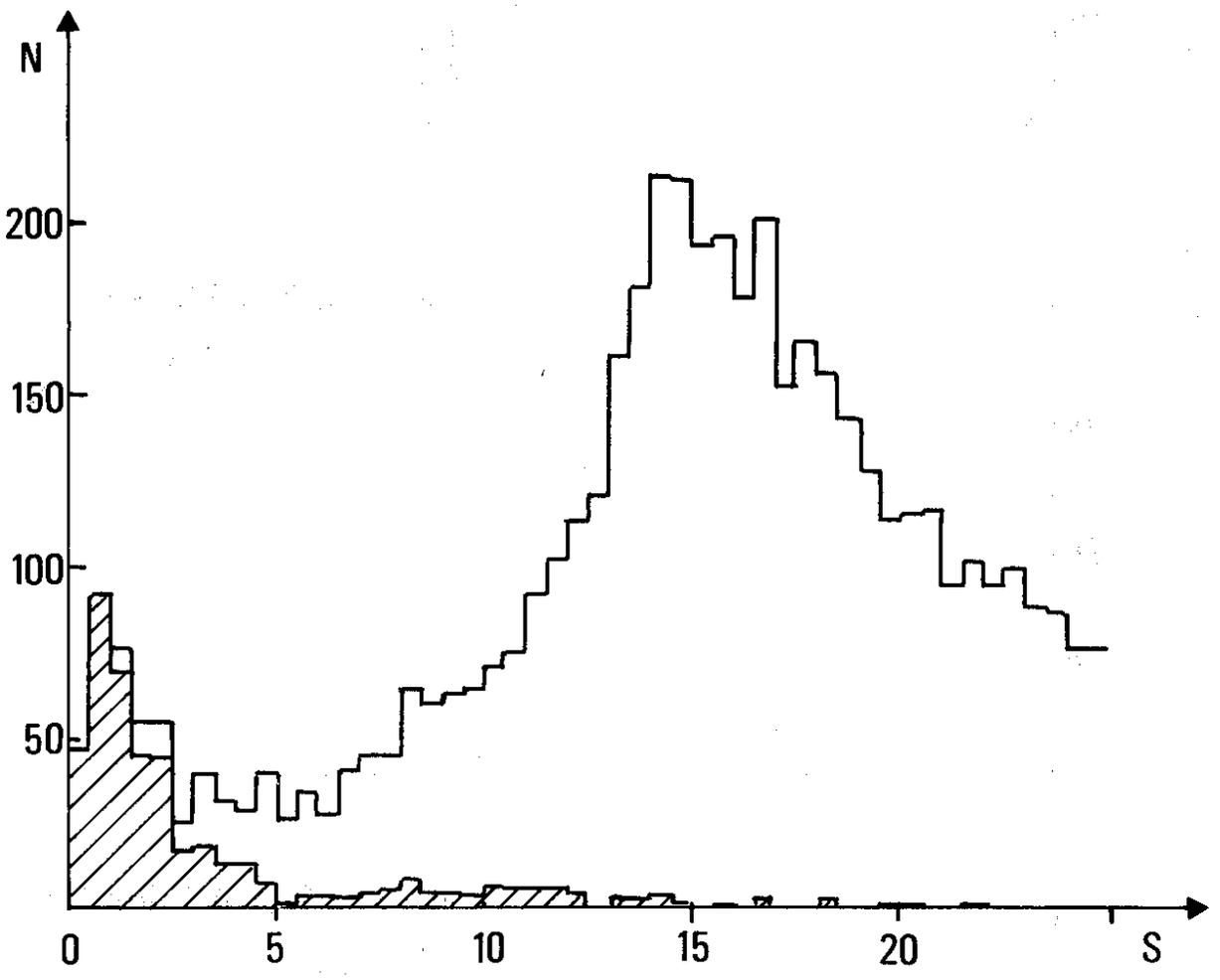

Fig. 11

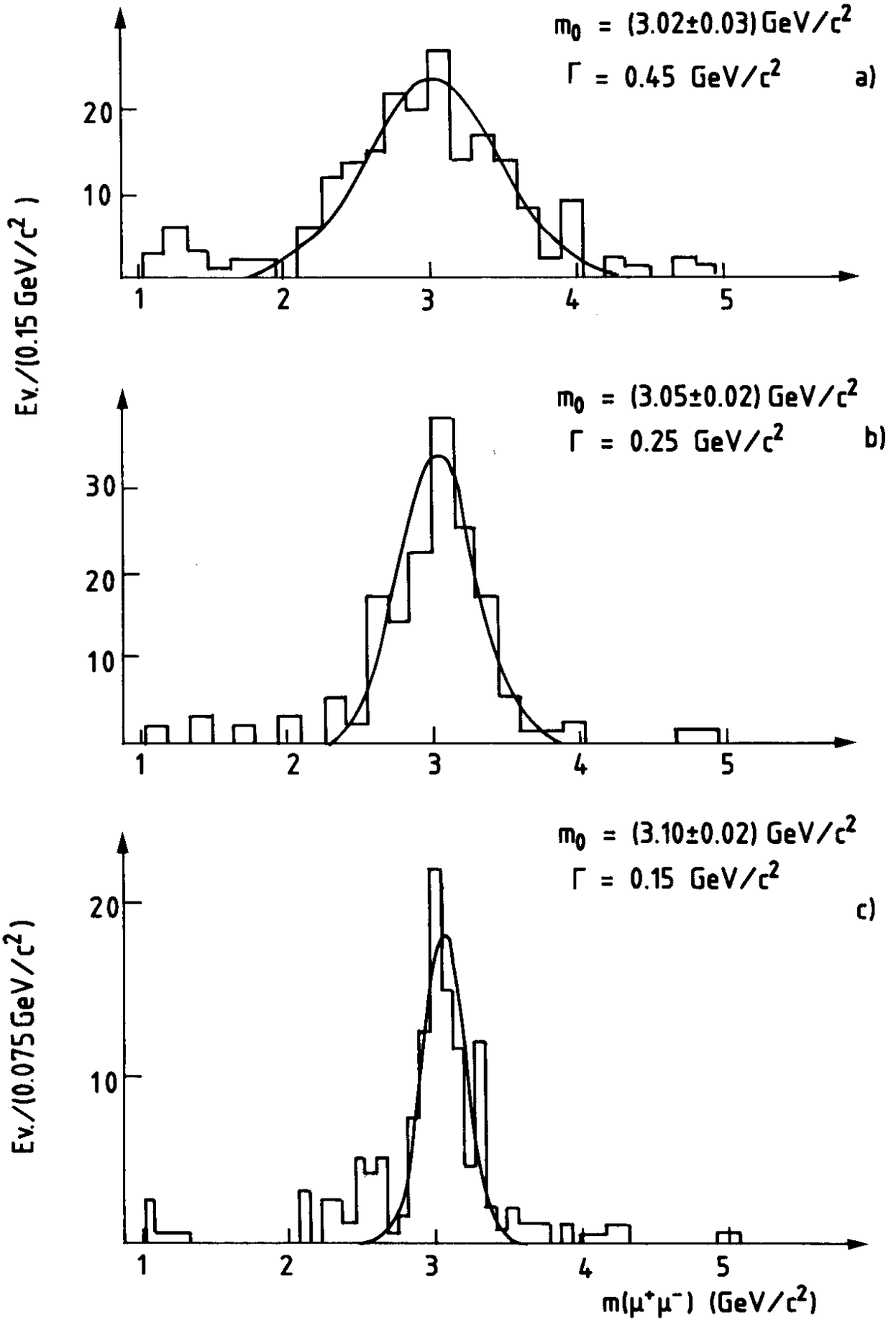
m_0 = (3.02±0.03) GeV/c^2
Γ = 0.45 GeV/c^2
a)
m_0 = (3.05±0.02) GeV/c^2
Γ = 0.25 GeV/c^2
b)
m_0 = (3.10±0.02) GeV/c^2
Γ = 0.15 GeV/c^2
c)
Ev./(0.15 GeV/c^2)
Ev./(0.075 GeV/c^2)
m($\mu^+\mu^-$) (GeV/c^2)

Fig. 12

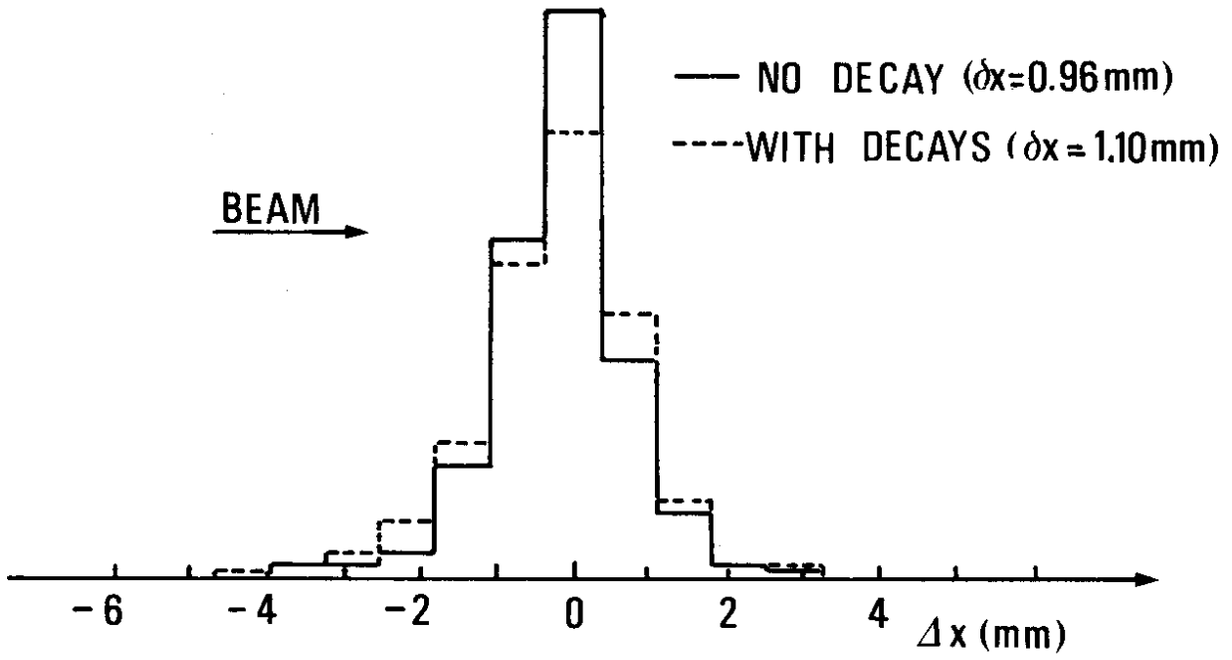
NO DECAY (δx=0.96mm)
WITH DECAYS (δx=1.10mm)
BEAM
-6
-4
-2
0
2
4
Δx (mm)

Fig. 13

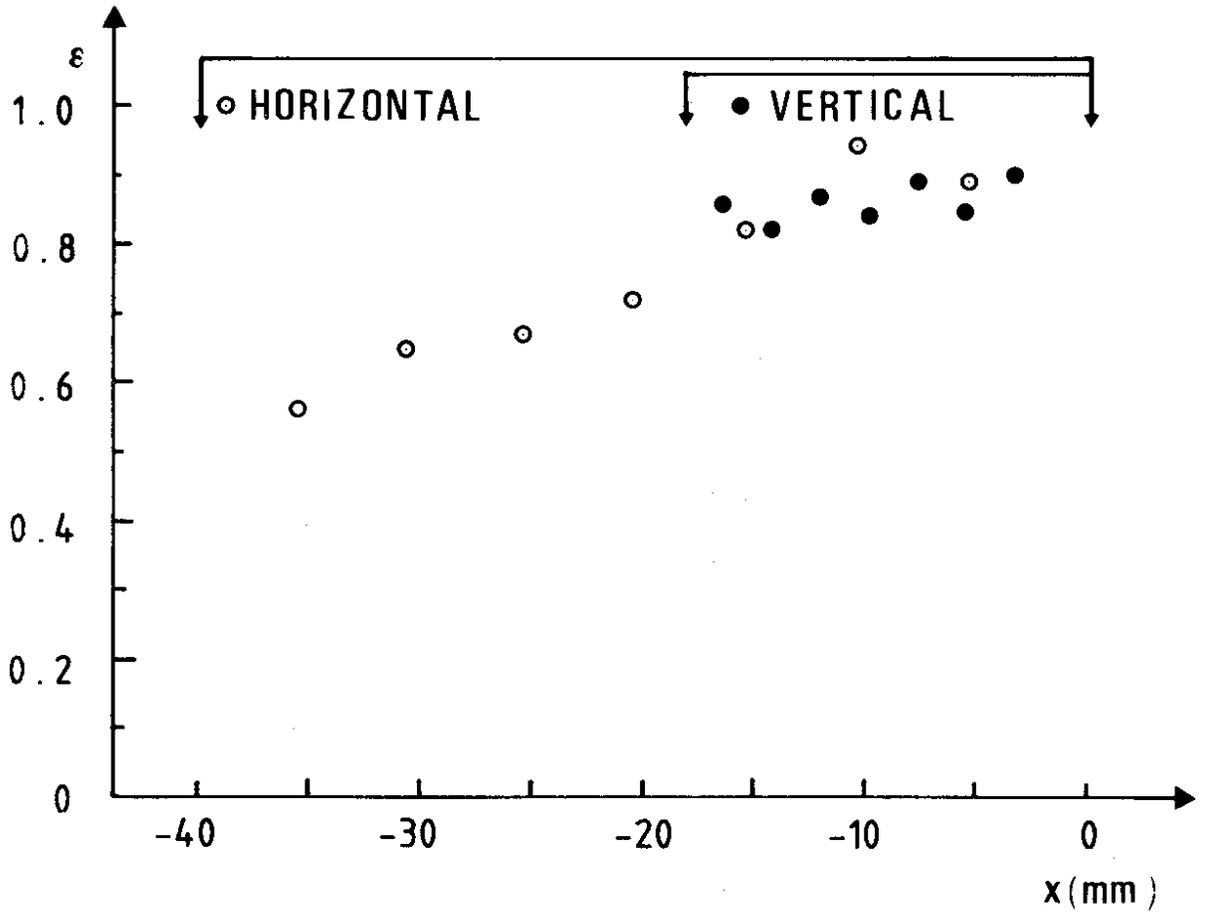
ε
HORIZONTAL
VERTICAL
1.0
0.8
0.6
0.4
0.2
0
-40
-30
-20
-10
0
x (mm)

Fig. 14

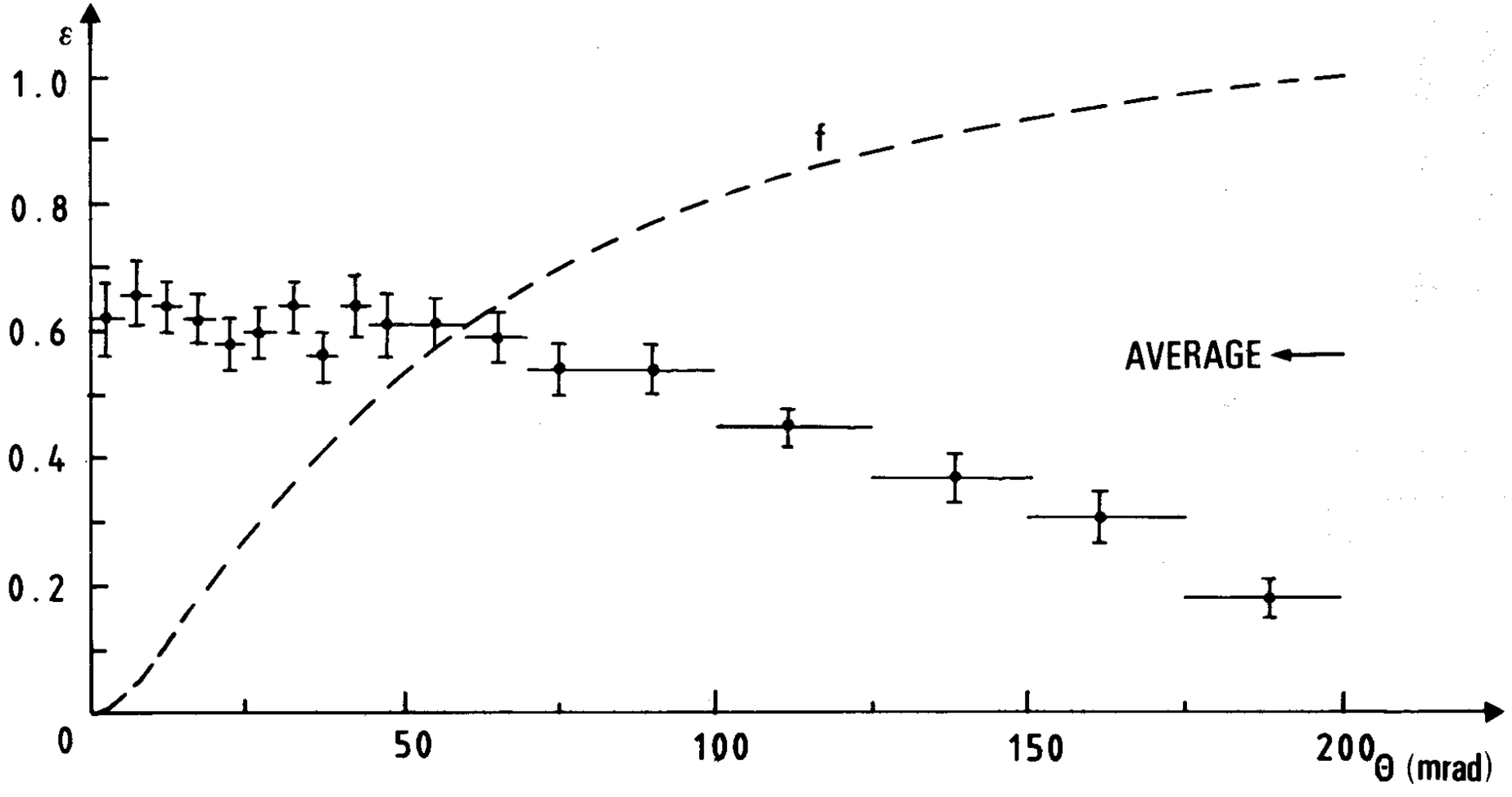

Fig. 15

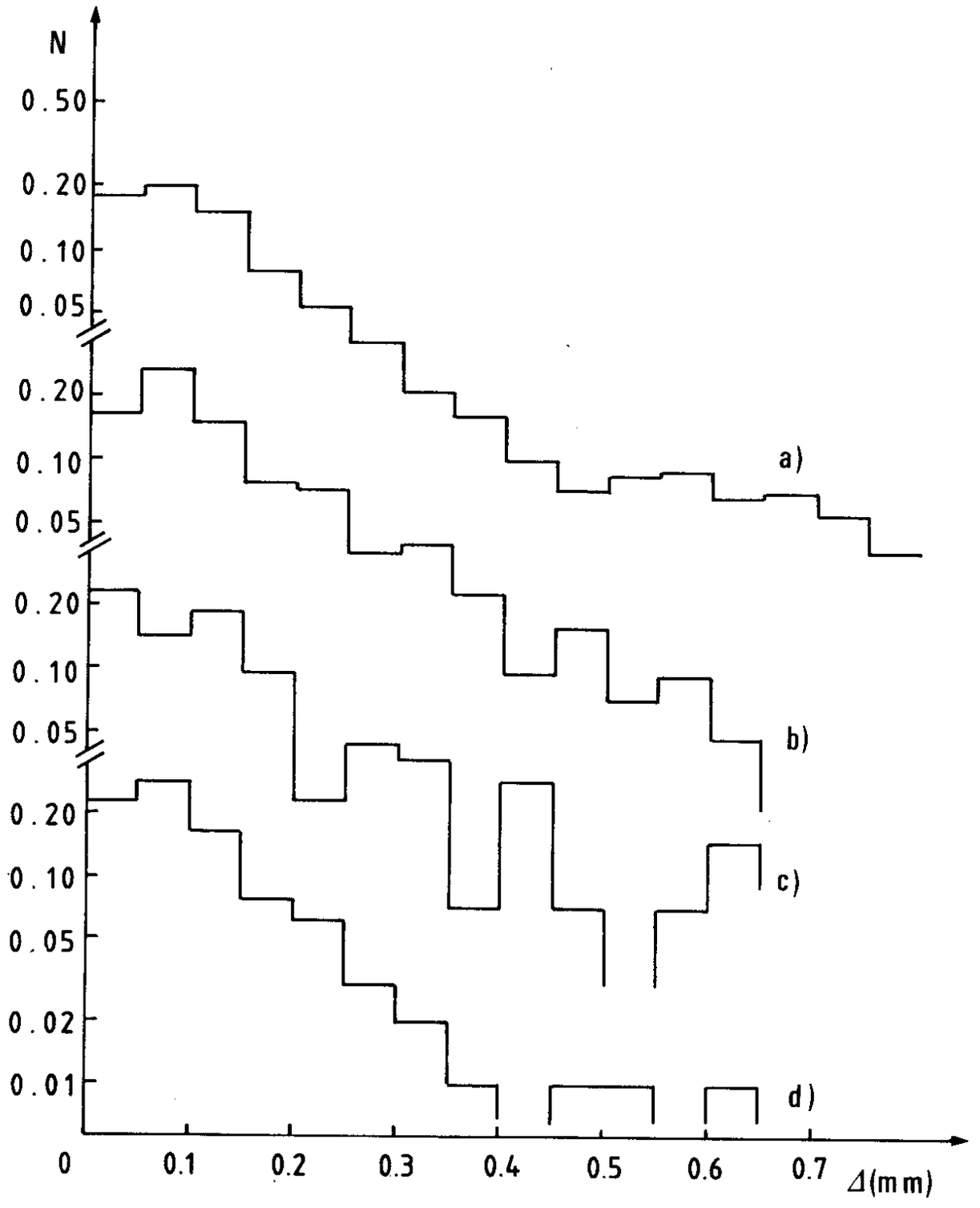
N
0.50
0.20
0.10
0.05
0.20
0.10
0.05
0.20
0.10
0.05
0.20
0.10
0.05
0.02
0.01
a)
b)
c)
d)
0
0.1
0.2
0.3
0.4
0.5
0.6
0.7
Δ(mm)

Fig. 16

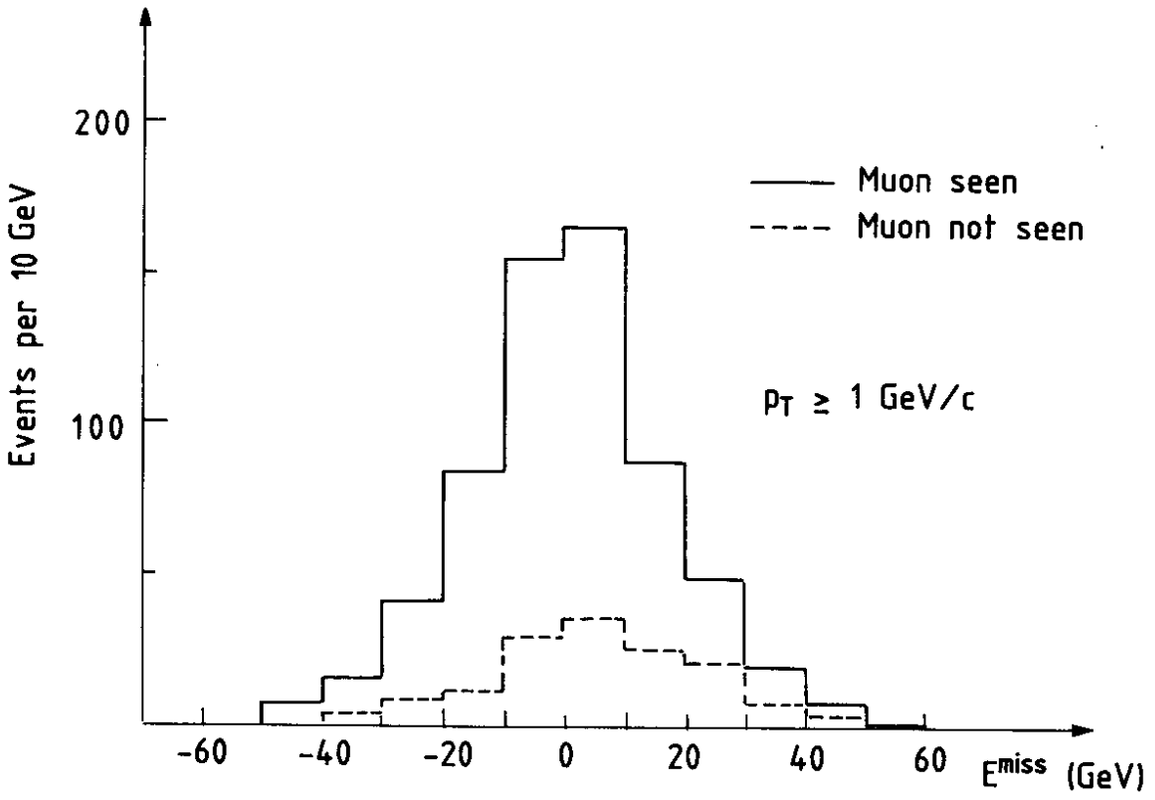
200
100
Events per 10 GeV
Muon seen
Muon not seen
$p_T \geq 1$ GeV/c
-60
-40
-20
0
20
40
60
E^{miss} (GeV)

Fig. 17

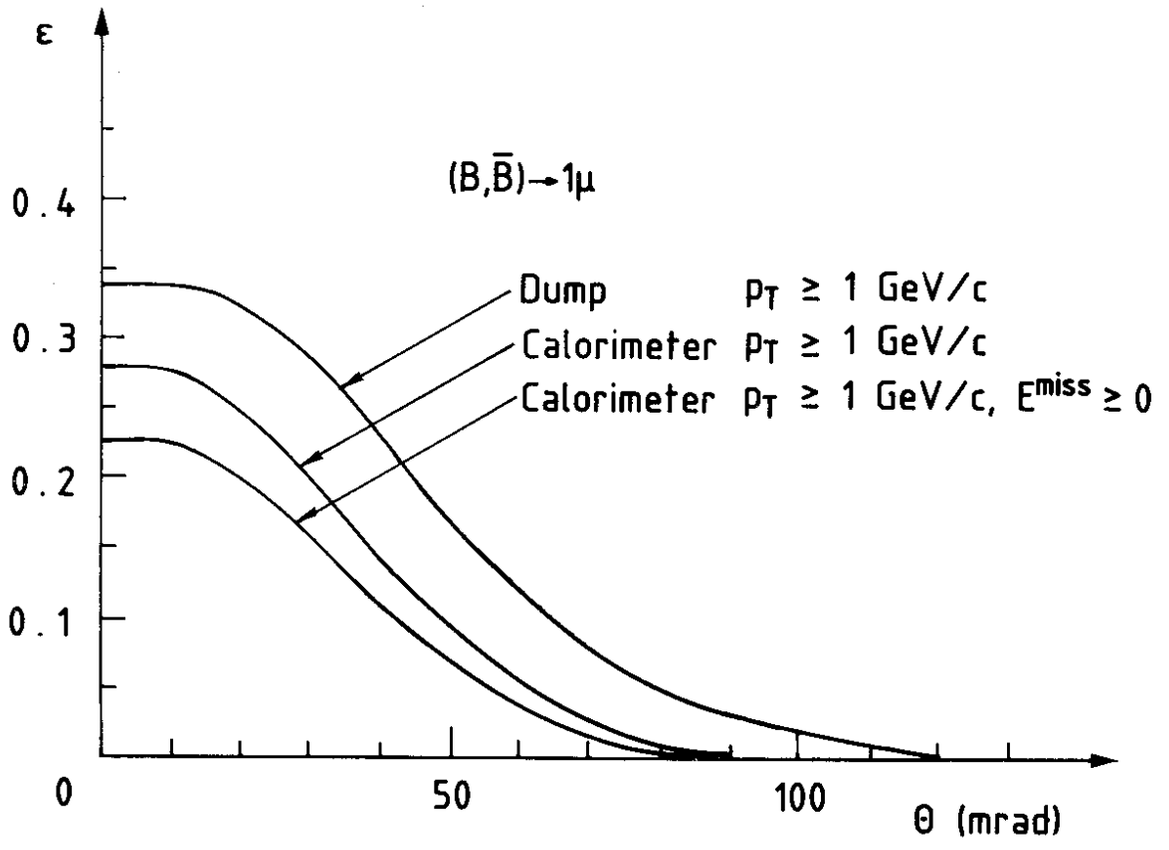
ε
$(B,\bar{B}) \rightarrow 1\mu$
0.4
0.3
0.2
0.1
0
Dump $p_T \geq 1$ GeV/c
Calorimeter $p_T \geq 1$ GeV/c
Calorimeter $p_T \geq 1$ GeV/c, $E^{miss} \geq 0$
50
100
θ (mrad)

Fig. 18

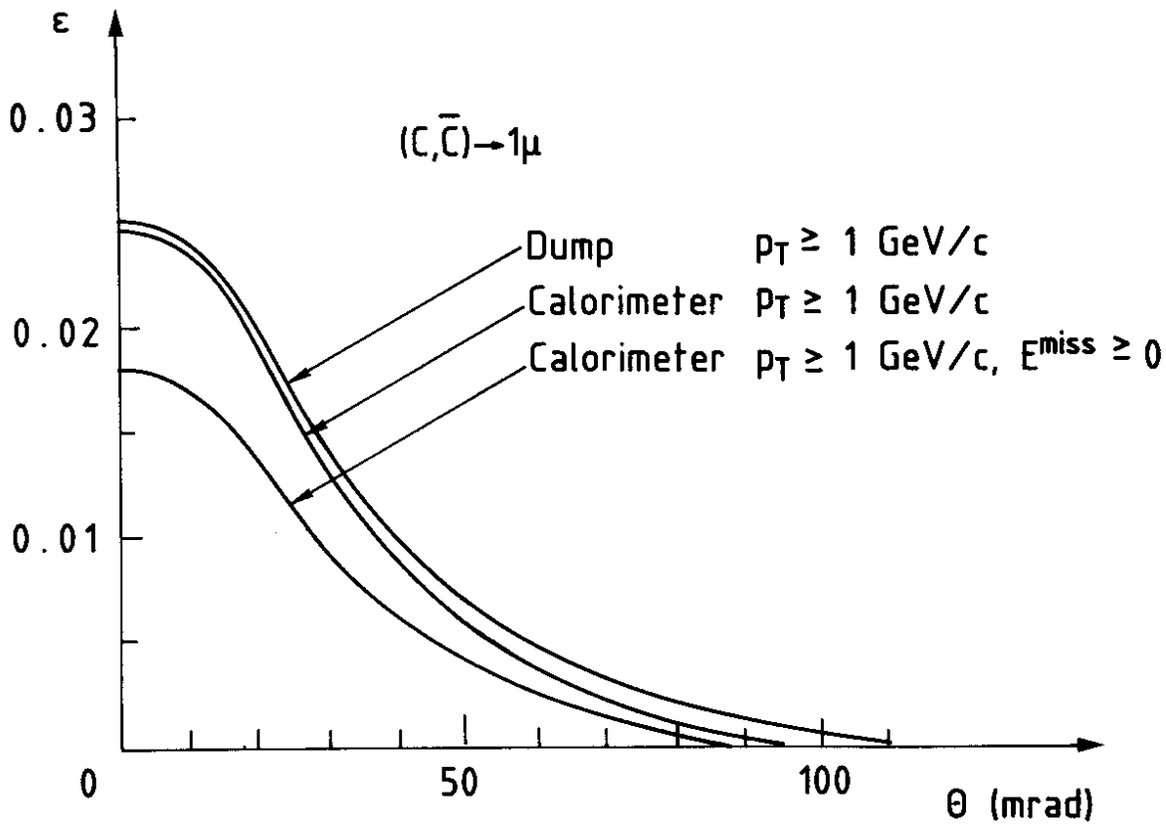
ε
0.03
0.02
0.01
0
50
100
Θ (mrad)
(C,C̄)→1μ
Dump
Calorimeter
Calorimeter
$p_T \geq 1$ GeV/c
$p_T \geq 1$ GeV/c
$p_T \geq 1$ GeV/c, $E^{miss} \geq 0$

Fig. 19